HHS Public Access

Author manuscript

Nature. Author manuscript; available in PMC 2019 September 27.

Published in final edited form as:

Nature. 2019 April ; 568(7750): 98–102. doi:10.1038/s41586-019-1066-x.

A gut-to-brain signal of fluid osmolarity controls thirst satiation

Christopher A. Zimmerman[1,2,3], **Erica L. Huey**[1,2,7], **Jamie S. Ahn**[1,2,8], **Lisa R. Beutler**[2,4], **Chan Lek Tan**[1,2,9], **Seher Kosar**[1,2], **Ling Bai**[1,2], **Yiming Chen**[1,2,3], **Timothy V. Corpuz**[1,2], **Linda Madisen**[6], **Hongkui Zeng**[6], and **Zachary A. Knight**[1,2,3,5]

[1]Department of Physiology, University of California, San Francisco, San Francisco, CA, USA

[2]Kavli Institute for Fundamental Neuroscience, University of California, San Francisco, San Francisco, CA, USA

[3]Neuroscience Graduate Program, University of California, San Francisco, San Francisco, CA, USA

[4]Department of Medicine, University of California, San Francisco, San Francisco, CA, USA

[5]Howard Hughes Medical Institute, University of California, San Francisco, San Francisco, CA, USA

[6]Allen Institute for Brain Science, Seattle, WA, USA

[7]Present: Graduate Program in Neuroscience, Harvard Medical School, Boston, MA, USA

[8]Present: California Northstate University College of Medicine, Elk Grove, CA, USA

[9]Present: Department of Neuroscience, Genentech Inc., South San Francisco, CA, USA

Satiation is the process by which eating and drinking reduce appetite. For thirst, oropharyngeal cues play a critical role in driving satiation by reporting to the brain the volume of fluid consumed[1–12]. In contrast, mechanisms that relay the osmolarity of ingested fluids remain poorly understood. Here we show that the water and salt content of the gastrointestinal (GI) tract are precisely measured and then rapidly communicated to the brain to control drinking behavior in mice. We demonstrate that this osmosensory signal is necessary and sufficient for satiation during normal drinking, involves the vagus nerve, and is transmitted to key forebrain neurons that control thirst and vasopressin secretion. Using microendoscopic imaging, we show that individual neurons compute homeostatic need by integrating this GI osmosensory information with oropharyngeal and bloodborne signals.

Correspondence and requests for materials should be addressed to Z.A.K. (zachary.knight@ucsf.edu).

Author Contributions

C.A.Z. and Z.A.K. conceived the project and designed the experiments. C.A.Z, E.L.H., and S.K. performed stereotaxic surgery. J.S.A. and L.R.B. performed intragastric surgery. J.S.A. performed vagotomy surgery. C.L.T. generated the *Nxph4-2a-Cre* mouse line. L.M. and H.Z. generated the *Ai148D* mouse line. C.A.Z., E.L.H., S.K., L.B., and Z.A.K. performed histology. E.L.H., J.S.A., and T.V.C. helped conduct experiments. Y.C. generated code. C.A.Z. conducted the experiments, analyzed the data, and generated the figures. C.A.Z. and Z.A.K. prepared the manuscript with input from all authors.

The authors declare no competing interests.

These findings reveal how the brain's fluid homeostasis system monitors the osmolarity of ingested fluids in order to dynamically control drinking behavior.

Drinking influences the volume and composition of the blood[1–4]. Yet ingestion of water and salt have opposing consequences for fluid balance, which raises the question of how the brain monitors the osmolarity of ingested fluids.

One way the brain controls drinking is by tracking the passage of fluids through the mouth and throat. Classic experiments demonstrated that drinking temporarily satiates thirst even if the ingested water is immediately drained from the esophagus[5–8], and recent work has identified specific populations of forebrain neurons that receive this rapid oropharyngeal signal during drinking[9–12]. This mechanism allows the brain to track fluid intake in real-time and thereby quench thirst and inhibit vasopressin secretion in anticipation of water absorption into the bloodstream, which occurs gradually over tens of minutes.

Nevertheless, this oropharyngeal signal communicates to the brain only the volume of fluid ingested, not its composition[9,12], which suggests that a distinct mechanism tracks fluid osmolarity during drinking. Taste aversion prevents the consumption of highly concentrated salt solutions[13,14], but there is little evidence that taste fine-tunes fluid consumption to match physiologic need. Infusion of fluids into the GI tract and hepatic portal circulation has been reported to influence drinking behavior and vasopressin secretion in some studies and species but not others[5–8,15–17], and it remains unclear where pre-absorptive fluids are monitored in the periphery, what exactly is sensed, which neurons in the brain receive this information, and how they use it to regulate behavior[1–4]. A fundamental source of ambiguity in these experiments is that traditional behavioral and physiologic readouts vary on the same timescale as fluid absorption (minutes), making it difficult to disentangle pre-absorptive signals that are sensed remotely in the periphery from systemic signals that are sensed directly in the brain.

To gain new insight into these longstanding questions, we set out to monitor directly the dynamics of thirst-promoting neurons in the brain while simultaneously manipulating the fluids ingested or infused into peripheral tissues. We first measured how fluid osmolarity influences drinking behavior and thirst neuron activity. Mice were equipped for fiber photometry recordings[18] of glutamatergic neurons in the subfornical organ[9,19,20] that promote drinking and directly monitor blood osmolarity (SFO^{Nos1} neurons; Fig. 1a). These animals were dehydrated and then given access to either water or hypertonic saline. As shown previously[9], ingestion of either fluid resulted in rapid inhibition of SFO^{Nos1} neurons that was time-locked to the act of drinking (Fig. 1b). SFO^{Nos1} neurons remained inhibited following bouts of water consumption, but their activity rebounded to an elevated, pre-ingestion level after each bout of saline consumption terminated (Fig. 1c). Based on the kinetics of this neural activity rebound, we hypothesized that SFO^{Nos1} neurons may receive a signal from the GI tract that depends on the osmolarity of the ingested fluid. Consistent with this, we found that isolated changes in GI osmolarity were sufficient to influence salt preference and drinking behavior (Extended Data Fig. 1).

To investigate how information about the water and salt content of the GI tract is communicated to the brain, we prepared mice with intragastric (i.g.) catheters for fluid infusion into the stomach[21] as well as fiber photometry implants for recording of SFO^{Nos1} neuron dynamics (Fig. 1d). Strikingly, i.g. infusion of water rapidly inhibited SFO^{Nos1} neurons (latency 105 ± 13 s, mean ± s.e.m.), whereas i.g. infusion of hypertonic saline activated the same population (Fig. 1e). Infusion of a range of NaCl concentrations revealed a remarkable linear correlation between the osmolarity of the infused fluid and the modulation of SFO^{Nos1} neuron activity (Fig. 1f). This response was independent of the initial hydration state of the animal (Fig. 1g) or the identity of the infused osmolyte (Extended Data Fig. 2), and was complete before any detectable change in blood osmolarity occurred (Extended Data Fig. 2), indicating that it reflects local sensing within the GI tract (likely in the proximal small intestine rather than the stomach itself) or hepatic portal circulation[3,15–17]. Consistent with this, infusion of hypertonic solutions strongly activated SFO^{Nos1} neurons regardless of whether the infused osmolyte could be absorbed into the bloodstream (Extended Data Fig. 2). Together, these data reveal that osmolarity is precisely measured within the GI tract and then communicated to thirst neurons in the brain.

We next investigated the significance of this gut-brain communication for thirst satiation. In dehydrated mice, i.g. infusion of water rapidly inhibited SFO^{Nos1} neurons (latency 107 ± 15 s, mean ± s.e.m.) and abolished drinking when water was subsequently presented (Fig. 2a,b and Extended Data Fig. 3). This indicates that changes in GI osmolarity (but not distension) are sufficient to satiate thirst and, conversely, that oropharyngeal cues are not required. The behavioral response to GI osmolarity changes (but not systemic changes) was hydration state-dependent: that is, i.g. infusion of salt did not stimulate drinking by animals that were hydrated but did cause an increase in water consumption by dehydrated animals (Fig. 2b,c and Extended Data Fig. 3). This state-dependent effect is reminiscent of how inhibition of satiation signals for feeding, such as cholecystokinin, can increase meal size in hungry animals but typically does not trigger the initiation of feeding in animals that are well-fed[22].

One mechanism by which GI osmolarity could regulate satiation is by acting as a “stabilization signal” that determines whether SFO^{Nos1} neurons remain inhibited when water drinking terminates (Fig. 1b,c). If this were true, then delivery of salt to the GI tract should cause SFO^{Nos1} neuron activity to rebound even after mice drink pure water. To test this, we gave dehydrated mice an i.g. infusion of salt and then analyzed the dynamics of SFO^{Nos1} neurons during early bouts of water drinking (Fig. 2d–f). Indeed, we found that the activity of SFO^{Nos1} neurons rebounded when drinking stopped, such that the neural dynamics during water ingestion now resembled those observed during hypertonic saline ingestion (Fig. 1b,c). This response was specific to salt infused into the stomach, as an identical dose of salt delivered by systemic injection produced no equivalent effect. This suggests that GI osmosensation specifies whether the rapid inhibition of thirst neurons by oropharyngeal cues during drinking is transient or durable.

We next investigated whether the inhibition of SFO neurons by the GI osmosensory signal is required for thirst satiation. We surgically equipped mice for i.g. infusion combined with simultaneous optogenetic activation[23] of SFO^{Nos1} neurons (Fig. 2g). As expected, brief (3 min) i.g. infusion of water into dehydrated mice eliminated drinking when water was

subsequently presented. However, optogenetic re-activation of SFO^{Nos1} neurons during and after water infusion completely blocked this satiating effect (Fig. 2h,i). This indicates that the SFO is a necessary site in the brain where the osmosensory signal from the GI tract is received to control the termination of drinking.

The peripheral mechanisms that communicate GI osmolarity to the brain are unknown. To begin to address this question, we investigated the role of the vagus nerve (cranial nerve X), which densely innervates the stomach and intestines[24]. Subdiaphragmatic vagotomy significantly attenuated the satiating effect of i.g. water infusion and, furthermore, greatly reduced the ability of i.g. water or salt to modulate SFO^{Nos1} neuron activity (Extended Data Fig. 4a–d). Genetic ablation of a subset of vagal sensory neurons had similar effects (Extended Data Fig. 4e–i). Together, these experiments indicate that vagal afferents are an essential part of the pathway by which GI osmolarity is communicated to the brain, although they do not rule out an additional role for circulating signals released from the gut following fluid ingestion.

We next investigated how information about the water and salt content of the GI tract is represented within the broader neural circuit that controls fluid homeostasis (Fig. 4a). We first recorded by fiber photometry the dynamics of vasopressin-secreting neurons in the supraoptic nucleus (SON^{Avp} neurons; Fig. 3a). We confirmed that, like SFO^{Nos1} neurons[9], these cells are activated by increases in blood osmolarity (Fig. 3b) and rapidly inhibited during drinking[7,10,25] (Fig. 3c). By combining i.g. infusions with neural recordings, we showed that SON^{Avp} neurons are also bidirectionally regulated by GI osmolarity with kinetics similar to SFO^{Nos1} neurons (Fig. 3d and Extended Data Fig. 5). This GI signal may function in coordination with oropharyngeal cues[10] to pre-emptively regulate vasopressin secretion during eating and drinking.

The median preoptic nucleus (MnPO) is a crucial node in the brain's fluid homeostasis system[1,2] that is bidirectionally connected to the SFO through glutamatergic neurons that promote drinking[11,12,26,27] (defined by expression of *Adcyap1*, *Agtr1a*, and *Nxph4*) and GABAergic neurons that inhibit drinking[12,26] (defined by expression of *Glp1r*). Given that this classification understates the heterogeneity of MnPO cell types[28] and that the single-cell dynamics of these neurons during behavior remain unknown, we used microendoscopic imaging[29] to investigate how these neurons encode aspects of fluid balance.

To gain genetic access to thirst-promoting, glutamatergic neurons in the MnPO, we generated knockin mice that express Cre recombinase from the *Nxph4* locus (*Nxph4-2a-Cre*; Fig. 4b and Extended Data Fig. 6). We then targeted GCaMP to these neurons and implanted a gradient-index lens above the MnPO in order to record their dynamics in awake, behaving mice (Fig. 4c). We first tested mice in a paradigm in which they were injected with isotonic saline, then 10 minutes later injected with salt to induce thirst, and then 10 minutes later given access to water (Fig. 4d,e). Analysis of neural dynamics in this paradigm by *k*-means clustering revealed three distinct subpopulations (Extended Data Fig. 7). One subpopulation (cluster 1, 17%) had no response to isotonic saline injection, but showed dramatic and sustained activation following salt challenge, suggesting that these neurons encode blood osmolarity. These same neurons were rapidly and uniformly inhibited during drinking. In

contrast, neurons from cluster 2 (34%) showed only transient responses that we interpret as likely representing stress or pain, whereas neurons from cluster 3 (49%) were largely unresponsive. We then investigated how these neurons respond to changes GI osmolarity. Intragastric infusion of water into dehydrated mice inhibited a subset of $MnPO^{Nxph4}$ neurons (24–26%), whereas infusion of hypertonic saline into hydrated mice activated a similar proportion of cells (34%; Fig. 4f,g and Extended Data Fig. 7). Registration of neurons across trials revealed that these two populations were largely overlapping, indicating that a specific subpopulation of $MnPO^{Nxph4}$ neurons is bidirectionally modulated by GI signals. Moreover, the majority of GI-tuned $MnPO^{Nxph4}$ neurons were robustly activated during thirst (Fig. 4h and Extended Data Fig. 7). This reveals that individual $MnPO^{Nxph4}$ neurons receive ingestion signals from the oropharynx, satiation signals from the GI tract, and homeostatic signals from the blood, which they integrate to estimate physiologic state. Experiments that combined chemogenetic silencing[30] with fiber photometry recordings suggest that these MnPO neurons are required for relaying GI osmolarity information to the SON, but not the SFO (Extended Data Fig. 8).

In contrast to $MnPO^{Nxph4}$ neurons, microendoscopic imaging of intermingled GABAergic MnPO neurons showed only weak and transient responses during salt challenge (Fig. 5a and Extended Data Fig. 9), indicating that these cells do not encode blood osmolarity in their baseline activity. We therefore recorded the dynamics of these neurons during water re-access after dehydration, which revealed strong responses during drinking (Fig. 5b–d and Extended Data Fig. 9). The majority of $MnPO^{Glp1r}$ neurons were either activated (28%) or inhibited (36%) during water ingestion; these responses were time-locked to the act of drinking, such that their activity returned to baseline when ingestion stopped. The cells exhibiting these varied responses were spatially intermingled (Fig. 5c), suggesting that the functional diversity of the MnPO is not anatomically organized at the scale of our recordings (500 μm). Of note, an earlier study using fiber photometry detected only activation of $MnPO^{Glp1r}$ neurons during drinking[12], which suggests that bulk fluorescence measurements masked the existence of an equal proportion of ingestion-inhibited cells. In addition, we observed smaller subsets of $MnPO^{Glp1r}$ neurons that were activated or inhibited by water access alone (Fig. 5b) or by i.g. infusion of either water or hypertonic saline (Fig. 5e–g and Extended Data Fig. 9). Together, these data indicate that the majority of GABAergic MnPO neurons are strongly modulated during ingestion, with smaller subsets encoding diverse signals relevant to fluid balance such as water availability, stress, and GI osmolarity.

Understanding how eating and drinking reduce appetite is one of the fundamental challenges in physiology. Traditionally, this problem has been studied by measuring the effect of peripheral manipulations on behavior[31,32]. Here, we have taken a complementary approach that uses the dynamics of appetite-promoting neurons in the brain as a readout to monitor in real-time the functional significance of manipulations to peripheral tissues. Using this strategy, we have shown that the water and salt content of the GI tract are precisely tracked during drinking and then communicated to the key neurons in the brain that control fluid balance. Furthermore, we have shown that this gut-to-brain signal requires the vagus nerve and is necessary and sufficient for the satiation of thirst and vasopressin secretion during normal behavior.

The GI osmosensory signal described here operates alongside oropharyngeal and bloodborne cues to regulate drinking behavior. We propose that these anatomically and temporally distinct signals cooperate to promote satiation in three steps (Extended Data Fig. 10). First, detection of liquid in the mouth generates a rapid signal that reports the volume of fluid ingested[9–12]. This early estimate of volume inhibits forebrain thirst neurons during the act of drinking, but is transient. Next, detection in the GI tract generates a second signal that reports the osmolarity of the ingested fluid. This early estimate of osmolarity stabilizes the inhibition of forebrain thirst neurons if water was consumed or causes their activity to rebound if the ingested fluid was hypertonic. Finally, absorption of water into the bloodstream alters fluid balance throughout the body, leading to sustained changes in well-characterized signals such as blood osmolarity that are monitored by the brain directly[1–4]. This three-step mechanism enables the brain to dynamically adjust drinking behavior to match the level of homeostatic need regardless of the composition of ingested fluids.

The concept of a “set point” or “balance point” has played a dominant role in shaping how we think about homeostasis[33,34]. Inherent in this concept is the idea that there is an anatomic site where measurements from the body are integrated to estimate the level of a physiologic variable. While this is commonly assumed to happen in specific neurons in the brain, it has rarely, if ever, been directly observed *in vivo*. We have shown here that individual, genetically defined thirst neurons in the MnPO integrate information about fluid balance arising from the oropharynx, GI tract, and blood. This reveals that homeostatic need can be computed at the level of single neurons in a living animal. Further study of this single-cell integration may provide new insight into the origin of the enigmatic set-points that characterize physiologic systems.

Methods

Experimental protocols were approved by the University of California, San Francisco IACUC following the NIH Guide for the Care and Use of Laboratory Animals.

Mouse strains

Adult mice (>6 weeks old) of both sexes were used for experiments. We obtained *Nos1-ires-Cre* knockin mice[35] (*Nos1*$^{tm1(cre)Mgmj}$/J, stock no. 017526), *Avp-ires2-Cre* knockin mice[36] (*Avp*$^{tm1.1(cre)Hze}$/J, stock no. 023530), *Glp1r-ires-Cre* knockin mice[37] (*Glp1r*$^{tm1.1(cre)Lbrl}$/J, stock no. 029283), *Rosa26-lsl-Gfp-Rpl10* knockin mice[38] (*Gt(ROSA)26Sor*$^{tm1(CAG-EGFP/Rpl10a,-birA)Wtp}$/J, stock no. 022367), and wild type mice (C57BL/6J, stock no. 000664) from the Jackson Laboratory. We obtained *Ai148D* GCaMP6f knockin mice[39] from the Allen Institute for Brain Science and *Trpv1-Gfp-2a-Dtr* BAC transgenic mice[40] from Mark Hoon at the National Institutes of Health.

We generated *Nxph4-2a-Cre* knockin mice by CRISPR/Cas9-mediated homologous recombination as previously described[27] based on published protocols[41,42]. Briefly, homology regions were captured into a plasmid from a BAC containing the *Nxph4* locus by recombineering. The T2A-Cre sequence was inserted immediately upstream of the endogenous stop codon. The final targeting vector contained ~3 kb (5′) and ~1.3 kb (3′) homology arms and was verified by restriction digest and sequencing. To generate site-

specific double stranded breaks using CRISPR, an sgRNA sequence (GAGTGAGACTGCGATCTGGT) was selected such that the guide sequence would be separated from the PAM site in the genomic DNA by the T2A-Cre insertion. This ensured that the targeting vector and recombined *Nxph4-2a-Cre* allele were protected from Cas9 nuclease activity. Super-ovulated female FVB/N mice were mated to FVB/N stud males, and fertilized zygotes were collected from oviducts. Cas9 protein (100 ng/μL), sgRNA (50 ng/μL), and targeting vector DNA (20 ng/μL) were mixed and injected into the pronucleus of fertilized zygotes. Injected zygotes were implanted into oviducts of pseudopregnant CD1 female mice. Founder pups and offspring were genotyped for the presence of the knockin allele by qPCR. Pups positive for the knockin allele were crossed to reporter mice, and reporter expression patterns were identical to endogenous *Nxph4* expression in the brain (Extended Data Fig. 6). All *Nxph4-2a-Cre* mice used here were maintained on a mixed FVB/C57Bl/6J background.

All mice were maintained in temperature- and humidity-controlled facilities with 12-h light–dark cycle with ad libitum access to water and standard chow (PicoLab 5053). *Avp-ires2-Cre;Ai148D* mice were fed doxycycline (80 mg/kg) chow (BioServ F7515) until undergoing stereotaxic surgery, after which they were fed standard chow. Mice were allowed at least two weeks for recovery after stereotaxic surgery before testing. For dehydration experiments, mice were water-deprived overnight (>16 h) before testing.

Viral vectors

We expressed channelrhodopsin-2 variants[43,44], GCaMP variants[45], and chemogenetic receptors[30] in genetically specified neurons by stereotaxic delivery of recombinant AAVs encoding Cre-dependent or *Camk2a*-promoter transgene cassettes. We obtained AAV1-CAG-FLEX-GCaMP6s, AAV5-Camk2a-GCaMP6f, and AAV5-hSyn-FLEX-GCaMP6f from the Penn Vector Core. We obtained AAV5-Camk2a-hChR2(E123T/T159C)-2a-mCherry and AAV5-Ef1a-DIO-hChR2(H134R)-mCherry from the UNC Vector Core. We obtained AAV5-hSyn-DIO-hM4D(G_i)-mCherry and AAV5-Camk2a-hM4D(G_i)-mCherry from Addgene.

Stereotaxic surgery

We performed intracranial surgery using stereotaxic coordinates for the SFO, MnPO, and SON[46] as previously described[9,27]. For delivery of recombinant AAVs, 100–200 nL of virus was injected (100 nL/min) at the SFO (−0.60 mm antero-posterior (AP), 0 mm medio-lateral (ML), −2.80 mm dorso-ventral (DV) relative to bregma) or MnPO (+0.35 mm AP, 0 mm ML, −4.20 mm DV). For SFO and MnPO photostimulation experiments, a Ø200 μm optical fiber (Thorlabs FT200UMT, CFLC230-10) was placed 0.30 mm above the injection site in the same surgery. For SFO fiber photometry experiments, a Ø400 μm optical fiber (Thorlabs BFH48-400, CF440-10) was placed 0.10 mm below the injection site in the same surgery. For SON fiber photometry experiments, a Ø400 μm optical fiber (Thorlabs BFH48-400, CF440-10) was placed unilaterally above the SON of *Avp-ires2-Cre;Ai148D* mice (−0.75 mm AP, −1.20 mm ML, −5.50 mm DV). For MnPO microendoscope imaging experiments, a Ø500 μm gradient-index (GRIN) lens (6.1 mm length; Inscopix 100-000588) was placed 0.10 mm above the injection site in the same surgery.

Optical fibers and GRIN lenses were then affixed to the skull using dental cement (A-M Systems 525000) or MetaBond adhesive cement (Parkwell S380). After at least two weeks recovery from the lens implantation surgery, mice to be used for microendoscope imaging were again anaesthetized and a baseplate (Inscopix 100-000279) was placed above the lens and affixed with MetaBond adhesive cement. When these mice were not being used for imaging, a baseplate cover (Inscopix 100-000241) was attached to prevent damage to the GRIN lens.

Intragastric surgery and infusion

We prepared mice for i.g. infusion as previously described[47] based on published protocols[21]. Briefly, catheters were constructed from Silastic tubing (Silastic 508-003), Tygon tubing (Tygon AAD04119), and a curved metal connector (Component Supply Company NE-9019). Biologically compatible mesh was attached to the Silastic tubing and around the metal connector using adhesive (Xiameter RTV-3110 base; Dow Corning 4 catalyst), and a luer adaptor (Instech LS20) was placed onto the Tygon tubing. Assembled catheters were sterilized using ethylene oxide. Mice with functional photometry, optogenetic, or microendoscope implants were anesthetized with ketamine/xylazine and the i.g. catheter was surgically implanted into the stomach as previously described[47]. Mice were allowed at least one week to recover prior to i.g. infusion and testing.

All i.g. infusions were delivered at a rate of 200 μL/min using a syringe pump (Harvard Apparatus 70-2001). Solutions of NaCl (75, 150, 250, 375, 500 mM), glucose (1 M), and mannitol (1 M) were prepared using deionized water, and 1.5 M NaCl solution was prepared using phosphate-buffered saline (PBS). Previous studies have indicated that mannitol is not absorbed into the bloodstream from the intestines[48]. We measured the latency for infused fluids to pass through the i.g. catheter itself en route to the stomach to be approximately 13 sec.

Vagotomy surgery

We prepared mice for i.g. infusion and performed bilateral subdiaphragmatic resection of the vagus nerve during a single procedure. Mice with functional photometry implants were anesthetized with ketamine/xylazine and the i.g. catheter was surgically implanted as described above. Briefly, a 5–7 mm incision was made along the medial line beginning at the distal edge of the sternum. Within a 3-mm radius around the incision site, the skin layer was separated from the muscular layer using blunt dissecting scissors. The liver was then retracted with sterile cotton swabs that had been moistened with saline so that the distal end of the esophagus could be visualized. Using jeweler’s forceps, both branches of the vagus nerve were isolated from the esophagus and a 1–2 mm section of each branch of the nerve was resected with scissors. Bilateral subdiaphragmatic vagotomy was accompanied in the same surgery by pyloroplasty, in which some of the muscle composing the pyloric sphincter was incised. Briefly, a 2-mm incision was made along the longitudinal axis of the pylorus without penetrating the lumen. Then each side of the incision was carefully approximated and sutured with two simple interrupted stitches. The purpose of the pyloroplasty is to maintain gastrointestinal flow through the pylorus[49] and thereby alleviate the excessive food retention, gastric distension, and morbidity that accompanies subdiaphragmatic vagotomy.

Control mice for vagotomy experiments underwent a sham surgery including i.g. catheter implantation and internal organ manipulation but not vagotomy or pyloroplasty.

To validate the subdiaphragmatic vagotomy, animals received an i.p. injection of wheat germ agglutinin conjugated to Alexa Fluor 555 (WGA-555; 200 μg per mouse) and were euthanized four days later. WGA-555 is taken up by axon terminals of intact vagal motor neurons[50], whose somas are located in the brainstem and can be visualized by histology (Extended Data Fig. 4a). Labeling in the dorsal motor nucleus of the vagus was greatly reduced, but not completely eliminated, by subdiaphragmatic vagotomy. Residual vagal fibers may be due to incomplete resection during the subdiaphragmatic vagotomy or to regeneration after surgery[51].

Behavior

We monitored mouse drinking behavior as previously described[9,27]. All experiments were performed in sound-isolated behavioral chambers (Coulbourn Habitest Modular System) and were performed during the light cycle to control for circadian factors. Fluid consumption was monitored with an electrical lickometer and recorded using Graphic State software (v4.2, www.coulbourn.com/category_s/363.html), or using LJStreamUD software during fiber photometry experiments (v1.17, www.labjack.com/support/software/applications/ud-series/ljstreamuid) or nVista software during microendoscope imaging experiments (v2.0, www.inscopix.com/nvista). Mice were acclimated to the behavioral chamber for at least 10 min at the beginning of each testing session.

For two-bottle drinking experiments (Extended Data Fig. 1d), wild type mice were dehydrated and then provided access to two randomly placed bottles (1× water, 1× 300 mM NaCl) for >10 min before being returned to their home cages. This test was repeated four times, with the location of the bottles randomly re-assigned on each trial. Mice were divided into two groups before testing. The first group received a gastric pre-load of hypertonic saline (1.5 M NaCl; 100 μL) by oral gavage one minute before bottle access; the second group received a gastric pre-load of isotonic saline (150 mM NaCl; 100 μL) by oral gavage one minute before bottle access.

For three-bottle drinking experiments (Extended Data Fig. 1e–g), SFO photometry mice were dehydrated and then provided access to three randomly placed bottles (1× water, 2× 300 mM NaCl) for >10 min before being returned to their home cages. This test was repeated four times, with the location of the bottles randomly re-assigned on each trial.

Fiber photometry

We prepared mice for *in vivo* fiber photometry recording as previously described[9] based on published protocols[18]. The fiber photometry signal was output to a lock-in amplifier (Stanford Research Systems SR810) with time constant 30 ms to allow filtering of noise at higher frequencies. The signal was then digitized (LabJack U6-Pro) and recorded using LJStreamUD software (v1.17, www.labjack.com/support/software/applications/ud-series/ljstreamuid) at 250 Hz sampling rate. Photometry data were subjected to minimal processing such as within-trial fluorescence normalization and temporal downsampling. For these experiments, i.g. infusions were given in a volume of 1 mL except for Fig. 2c–f and

Extended Data Fig. 2h (volume of 200 μL, including ~50 μL dead volume); systemic (i.p.) injections were given in a volume of 150 μL (1.5 M or 3 M NaCl) using PBS as "vehicle" or in a volume of 1 mL (water); oral gavages (Extended Data Fig. 8) were given in a volume of 150 μL. Hormones (Extended Data Fig. 4i) were delivered by i.p. injection (volume of 150 μL) for serotonin (2, 20 mg/kg), cholecystokinin (2 mg/kg), ghrelin (2 mg/kg), and leptin (2 mg/kg) and by subcutaneous injection (volume of 400 μL) for amylin (2 mg/kg) using PBS as "vehicle".

Microendoscope imaging

We prepared mice for *in vivo* microendoscope imaging based on published protocols[29,52]. Videos were acquired at 20 Hz (20% LED power, 2.0 gain) using a miniature microscope (Inscopix) and nVista software (v2.0, www.inscopix.com/nvista). After acquisition, videos were first pre-processed, spatially (binning factor of 2) and temporally (binning factor of 5) downsampled, and motion-corrected using Mosaic software (v1.7, support.inscopix.com/mosaic-workflow). Activity traces for individual neurons were then extracted from these videos using the constrained nonnegative matrix factorization (CNMF-E) pipeline[53] (www.github.com/zhoupc/cnmf_e) implemented in Matlab. After initial CNMF-E segmentation, extracted neurons were manually refined to avoid potential confounds from uncorrected motion artifacts, ROI duplication, and over-segmentation of the same spatial components. For each experiment, activity traces for individual neurons were extracted from recordings from 3–4 mice and then pooled for subsequent analysis. For these experiments, i.g. infusions were given in a volume of 1 mL; systemic (i.p.) injections were given in a volume of 100 μL (3 M NaCl) using PBS as "vehicle".

Optogenetics

We prepared mice for *in vivo* photostimulation as previously described[9,27] based on published protocols[23,54]. A DPSS 473 nm laser (Shanghai Laser and Optics Century BL473-100FC) was controlled by Graphic State software (v4.2, www.coulbourn.com/category_s/363.html) through a TTL signal generator (Coulbourn H03-14) and synchronized with behavior experiments. The laser power was measured to be ~15 mW at the patch cable tip and was delivered in 10-ms pulses at 20 Hz. For these experiments, i.g. infusions were given in a volume of 600 μL.

Chemogenetics

We prepared mice for *in vivo* chemogenetic inhibition based on published protocols[55,56]. Clozapine *N*-oxide (CNO, 1 mg/kg) was delivered by i.p. injection (volume of 125 μL) with 0.6% DMSO in PBS as "vehicle". For these experiments (Extended Data Fig. 8), CNO or vehicle was delivered >15 min before water access after dehydration or oral gavage of hypertonic NaCl.

Diphtheria toxin receptor ablation

We ablated genetically defined (*Trpv1*$^{+}$) sensory neurons using the DTX receptor-based strategy described in published protocols[40,57]. Briefly, *Nos1-ires-Cre;Trpv1-Gfp-2a-Dtr* mice were first equipped for fiber photometry recording of SFO neurons and screened for

functionality. Mice with functional photometry implants then underwent i.g. catheterization surgery and, after recovery, were tested in a series of experiments ("before DTX" in Extended Data Fig. 4h,i). Mice were then given two intramuscular injections of DTX (each injection was 50 μL of 25 μg/mL DTX) separated by three days and then allowed at least five additional days to recover, after which they underwent the same series of experiments ("after DTX").

We confirmed the ablation of *Trpv1*$^+$ sensory neurons in two ways. First, *Nos1-ires-Cre;Trpv1-Gfp-2a-Dtr* photometry/i.g. mice were given access to a single bottle of palatable sugar solution (300 mM sucrose) that also contained either capsaicin (100 μM) or vehicle (0.15% TWEEN-80 + 1.5% DMSO). This test was conducted once before and once after DTX treatment, and intake was quantified from 1–2 h after access (Extended Data Fig. 4h). Second, *Trpv1-Gfp-2a-Dtr;hSyn-Nanobody-Rpl10* mice were used for histology of the nodose ganglion and thoracic dorsal root ganglion (DRG) after either DTX treatment or no treatment. This revealed nearly complete ablation of *Trpv1*$^+$ vagal neurons and more limited ablation of *Trpv1*$^+$ DRG neurons (Extended Data Fig. 4e,f). We also observed sparse labeling of *Trpv1*$^+$ neurons in the brain[58], and this was unaffected by DTX treatment (Extended Data Fig. 4g).

Plasma osmolality

Mice equipped with i.g. catheters were fully hydrated and received an infusion (sham, water, 150 mM NaCl, or 500 mM NaCl) at 200 μL/min for 5 min. Beginning 3 min after the start of infusion, 125 μL of blood was collected from the tail vein using EDTA-coated capillary tubes (RAM Scientific 07-6011). The blood collection process took approximately 3 min per mouse. Plasma was isolated by centrifugation (1000 g for 10 min), diluted in deionized water, and frozen until measurement. Osmolality was then measured in triplicate for each sample using a freezing point osmometer (Fiske Associates 210). Mice were allowed one week for recovery between sessions.

Histology

Mice were transcardially perfused with PBS followed by 10% formalin. To visualize forebrain and hindbrain nuclei, whole brains were dissected, post-fixed in 10% formalin overnight at 4°C, and then cryo-protected in 30% sucrose overnight at 4°C. Free-floating sections (40 μm) were prepared with a cryostat, blocked (3% BSA, 2% NGS, and 0.1% Triton-X in PBS for 2 h), then incubated with primary antibody (chicken anti-GFP, Abcam ab13970, 1:1000; rat anti-RFP, ChromoTek 5f8, 1:1000; goat anti-mCherry, Acris ab0040-200, 1:1000; rabbit anti-Fos, Santa Cruz Biotech sc52, 1:500) overnight at 4°C. Sections were then washed, incubated with secondary antibody (Alexa Fluor 488 goat anti-chicken, Life Technologies a11039, 1:1000; Alexa Fluor 568 goat anti-rat, Life Technologies a11077, 1:1000; Alexa Fluor 568 goat anti-rabbit, Life Technologies a11011, 1:1000; Alexa Fluor 568 donkey anti-goat, Life Technologies a11057, 1:1000) for 2 h at room temperature, washed again, mounted with DAPI Fluoromount-G (Southern Biotech), and then imaged with a confocal microscope (Zeiss LSM-700). To visualize WGA-555 labelling of the dorsal motor nucleus of the vagus, sections were mounted and imaged without staining.

To visualize sensory ganglia, the ventral aspects of the skull and vertebral columns were dissected, post-fixed in 10% formalin overnight at 4°C, and then washed at room temperature. The nodose ganglion and thoracic DRG were further dissected and then cryo-protected in 30% sucrose overnight at 4°C. Sections (20 μm) were prepared with a cryostat, mounted on slides, washed, blocked (5% NGS and 0.1% Triton-X in PBS for 30 min), and then incubated with primary antibody (chicken anti-GFP, Abcam ab13970, 1:1000; rabbit anti-NeuN, Milliipore abn78, 1:1000) overnight at 4°C. Sections were then washed, incubated with secondary antibody (Alexa Fluor 488 goat anti-chicken, Life Technologies a11039, 1:500; Alexa Fluor 568 goat anti-rabbit, Life Technologies a11011, 1:500) for 2 h at room temperature, washed again, mounted with DAPI Fluoromount-G (Southern Biotech), and then imaged with the confocal microscope.

Images underwent minimal processing, such as brightness and contrast adjustments, performed using the Fiji distribution of ImageJ (v2.0, www.fiji.sc).

Data analysis

We analyzed behavior data, fiber photometry data, and microendoscope imaging data using custom Matlab (vR2018a, www.mathworks.com/products/matlab) scripts. Throughout the paper, a drinking bout is defined as any set of ten or more licks in which no inter-lick interval is greater than one second. For some assays, multiple trials of the same experiment were performed for an individual mouse and then averaged and treated as a single replicate. For photometry data, all responses were normalized using the function: $\Delta F/F_0 = (F–F_0)/F_0$, in which F is the raw photometry signal and F_0 is the median of F during the baseline period (plotted data before injection/infusion/drinking). For quantification in bar graphs, the median $\Delta F/F_0$ of a 10-s (for long experiments with >5 min of data plotted) or 2-s (for short experiments with <5 min of data plotted) window is reported. For peri-event time histograms around the end of drinking bouts, F_0 was defined as the median of F at the time (±1 s) of the last lick in the bout. For microendoscope imaging data, all responses were normalized using the function $z = (C_{raw}–\mu)/\sigma$, in which C_{raw} is the output of the CNMF-E pipeline, μ is the mean of C_{raw} during the baseline period, and σ is the standard deviation of C_{raw} during the baseline period. *k*-means clustering was performed using the built-in Matlab function (www.mathworks.com/help/stats/kmeans.html) as illustrated in Extended Data Fig. 7a. For quantification in linear regressions, the mean *z*-score of the final 1 min of plotted data for i.g. infusions (9–10 min after infusion begins) or of the first 1 min after drinking onset (first lick in first bout) is reported. The mean *z*-score of the first 1 min after the first lick in the first drinking bout was used to classify GABAergic MnPO neuron responses during ingestion (Fig. 5c,d and Extended Data Fig. 9b,c). For time-courses of water intake, time 0 is the moment of water access unless otherwise noted. Initial drinking rate (Fig. 2b) was calculated from the first 1 min of drinking after the first lick in the experiment. Latency to inhibition of SFO^{Nos1}neurons by i.g. infusion of water (main text) was calculated as the moment at which the fiber photometry signal crossed a threshold of four standard deviations (4σ) below the signal level during the baseline period and was adjusted to account for the dead volume of the i.g. catheter.

Statistics and reproducibility

We performed statistical analyses using Prism (v7.0, www.graphpad.com/scientific-software/prism). Throughout the paper, values are reported as mean ± s.e.m. (error bars or shaded area). In figures with linear regressions, the shaded area represents the 95% confidence interval for the line-of-best-fit. *P*-values for pair-wise comparisons were performed using a two-tailed Student's *t*-test (with repeated measures when possible). *P*-values for comparisons across multiple groups were performed using ANOVA (with repeated measures when possible) and corrected for multiple comparisons using the Holm-Šídák method (within-group comparison to the control condition). $*P < 0.05$, $**P < 0.01$, $***P < 0.001$, $****P < 0.0001$. Randomization, blinding, and statistical methods to predetermine sample size were not used. Representative images were selected from one to five original biological replicates, and representative recordings were selected from three to five original biological replicates. Representative mouse brain schematics (coronal and sagittal sections) were adapted from ref. [46]. More information about statistics and reproducibility is available in the online Reporting Summary.

Code availability

Custom Matlab scripts that support the findings of this study are available upon reasonable request the corresponding author.

Data availability

Data that support the findings of this study are available upon reasonable request the corresponding author.

Extended Data

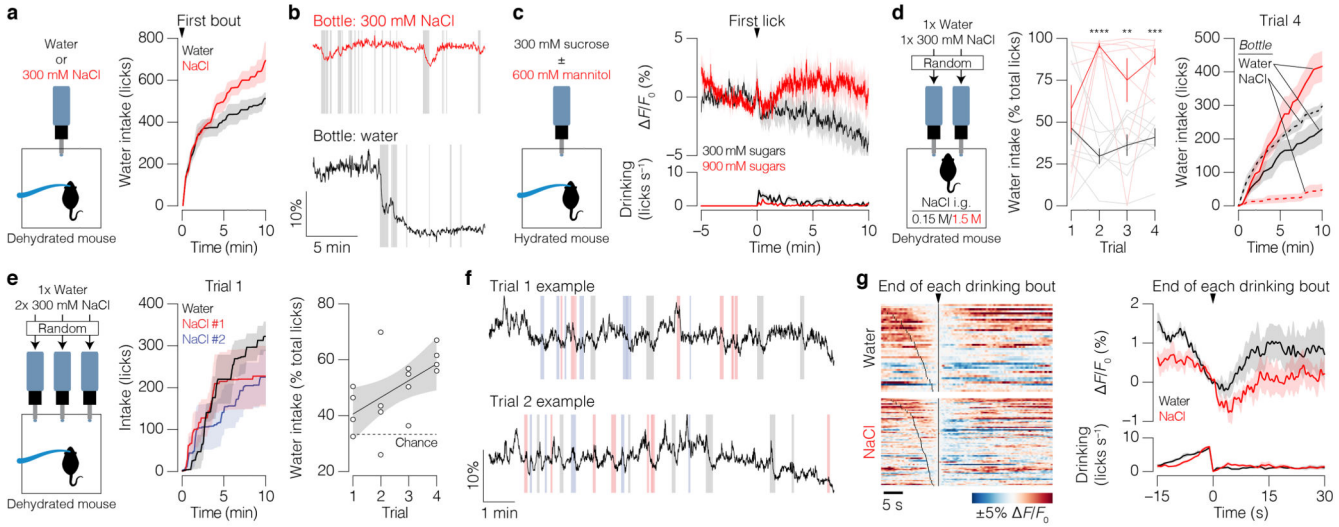

Extended Data Figure 1. GI osmolarity influences drinking behavior and biases salt preference.

Panels **a,b** present additional data related to Fig. 1b,c. **a,** Cumulative water or 300 mM NaCl intake after dehydration (n = 5 mice). **b,** Example SFO neuron dynamics during drinking after dehydration. Panel **c** shows that ingestion of hypertonic fluids activates SFO neurons regardless of hydration state. **c,** Average SFO activity and drinking behavior of hydrated mice given *ad libitum* access to isotonic (300 mM sucrose) or hypertonic (300 mM sucrose + 600 mM mannitol) sugar solutions of similar sweetness (n = 5 mice). Panel **d** shows that increases in GI osmolarity bias salt/water preference. **d,** Preference in a two-bottle test after i.g. treatment with hypertonic (red; n = 8 mice) or isotonic (black; n = 9 mice) NaCl (left; two-way ANOVA, Holm-Šídák correction). Cumulative water (solid lines) and 300 mM NaCl (dashed lines) intakes in the same two-bottle test (right). Panels **e–g** show that post-ingestive SFO neuron activity does not reflect the delayed consequences of taste or sensorimotor experience associated with an individual drinking bout. **e,** Mice initially do not distinguish between bottles containing water or 300 mM NaCl in a three-bottle test after dehydration (n = 4 mice, linear regression, R^2 = 0.3163, P = 0.0233). **f,** Example SFO neuron dynamics during drinking from water (black) and 300 mM NaCl (blue, red) bottles after dehydration. **g,** SFO neuron dynamics during individual water (42 bouts) or NaCl (71 bouts) drinking bouts in trials 1 and 2 of the three-bottle test (left). Average SFO activity after individual drinking bouts (right; n = 4 mice). In this experiment (panels **e–g**), GI osmolarity quickly becomes hypertonic as the dehydrated mice alternate between drinking from water and NaCl bottles such that SFO neuron activity "rebounds" even after water drinking bouts, which suggests that the stabilization signal that either quenches or re-activates SFO neurons after ingestion reflects GI osmolarity. Error bars represent mean ± s.e.m. Shaded areas in **a,c,d,e,g** represent mean ± s.e.m.; in **b** represent individual licks; in the linear regression (right) in **e** represent 95% confidence interval of the line-of-best-fit; in **f** represent individual drinking bouts. $^{**}P < 0.01$, $^{***}P < 0.001$.

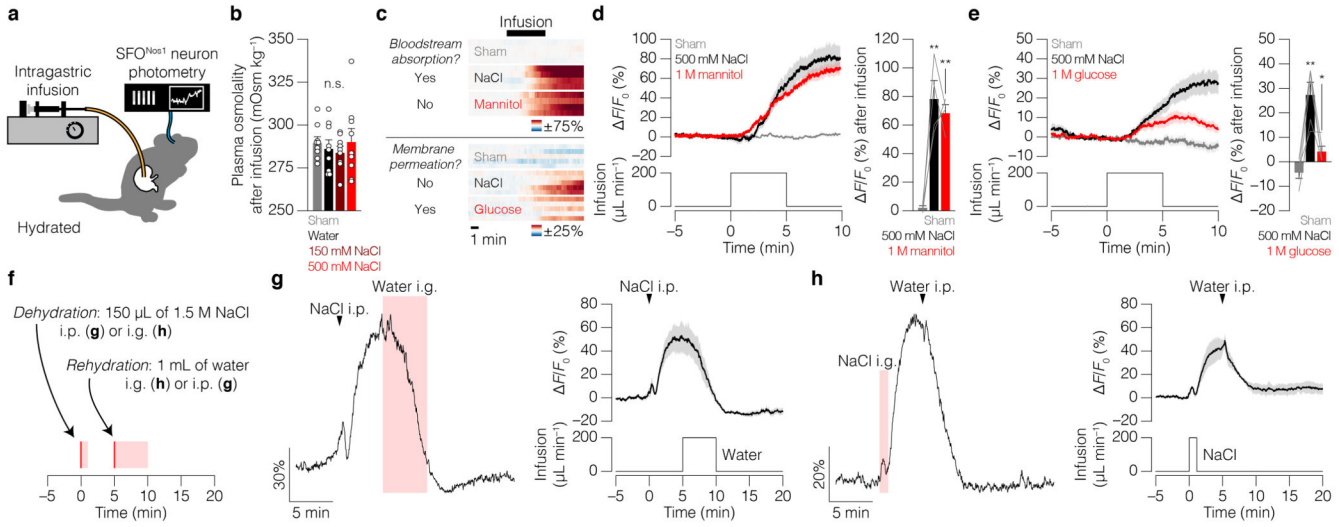

Extended Data Figure 2. The GI→SFO osmosensory signal depends on fluid tonicity but not osmolyte identity.

Panels **a,b** show that i.g. infusion does not rapidly alter the state of the blood. **a,** Schematic. **b,** Plasma osmolality of samples collected during approximately 3–6 min after the start of the 5-min i.g. infusion ($n = 9$ mice per group, one-way ANOVA, Holm-Šídák correction). Panels **c–e** show that the GI→SFO osmosensory signal depends on fluid tonicity but not osmolyte identity. **c,** SFO neuron dynamics of individual mice in response to i.g. infusion of equiosmotic concentrations of NaCl, which is absorbed into the bloodstream from the GI tract, and mannitol, which is not absorbed (top; $n = 4$ mice). SFO neuron dynamics of a separate cohort of individual mice in response to i.g. infusion of equiosmotic concentrations of NaCl, which does not permeate cell membranes and has high tonicity, and glucose, which does permeate cell membranes and has low tonicity (bottom; $n = 5$ mice). **d,** Average SFO activity during i.g. infusion of NaCl or mannitol (left). Quantification (right; $n = 4$ mice, one-way ANOVA, Holm-Šídák correction). **e,** Average SFO activity during i.g. infusion of NaCl or glucose (left). Quantification (right; $n = 5$ mice, one-way ANOVA, Holm-Šídák correction). Panels **f–h** show that SFO neurons encode systemic and GI osmosensory signals additively rather than hierarchically. **f,** Schematic. **g,** Example (left) and average (right; $n = 4$ mice) SFO neuron dynamics during 1.5 M NaCl i.p. injection followed by water i.g. infusion. **h,** Example (left) and average (right; $n = 3$ mice) SFO neuron dynamics during 1.5 M NaCl i.g. infusion followed by water i.p. injection. Error bars represent mean ± s.e.m. Shaded areas in summary traces (**d,e,g,h**) represent mean ± s.e.m. and in example traces (**g,h**) represent i.g. infusion. $*P < 0.05$, $**P < 0.01$; n.s., not significant.

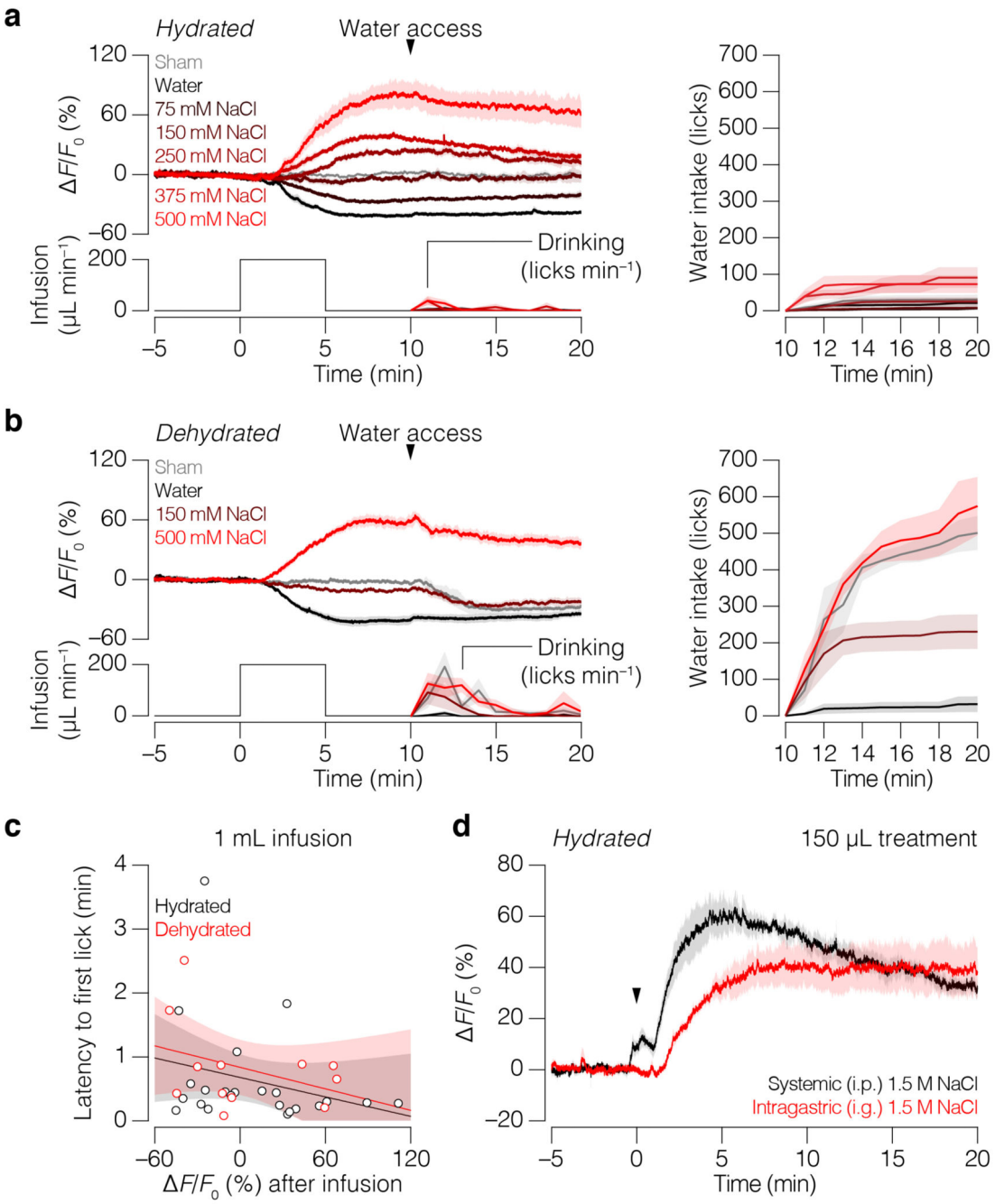

Extended Data Figure 3. The GI→SFO osmosensory signal completely satiates but only mildly stimulates thirst.

Panels **a,b** present additional data related to Fig. 1e–g and Fig. 2a,b. **a,** Average SFO activity during i.g. infusions and subsequent drinking while hydrated (left). Cumulative water intake (right; $n = 4$ mice). **b,** Average SFO activity during i.g. infusions and subsequent drinking after dehydration (left). Cumulative water intake (right; $n = 4$ mice). **c,** Correlation between SFO activity change and latency to drinking after 1 mL infusions into hydrated (black; $n =$ 23 experiments from 4 mice, linear regression, $R^2 = 0.0705$, $P = 0.2208$) or dehydrated (red;

n = 12 experiments from 4 mice, linear regression, R^2 = 0.1321, *P* = 0.2456) mice. Panel **d** presents additional data related to Fig. 2c. **d,** Average SFO activity after systemic (i.p.) or i.g. treatment with 150 μL NaCl while hydrated. Shaded areas in **a,b,d** represent mean ± s.e.m. and in **c** represent 95% confidence interval of the line-of-best-fit.

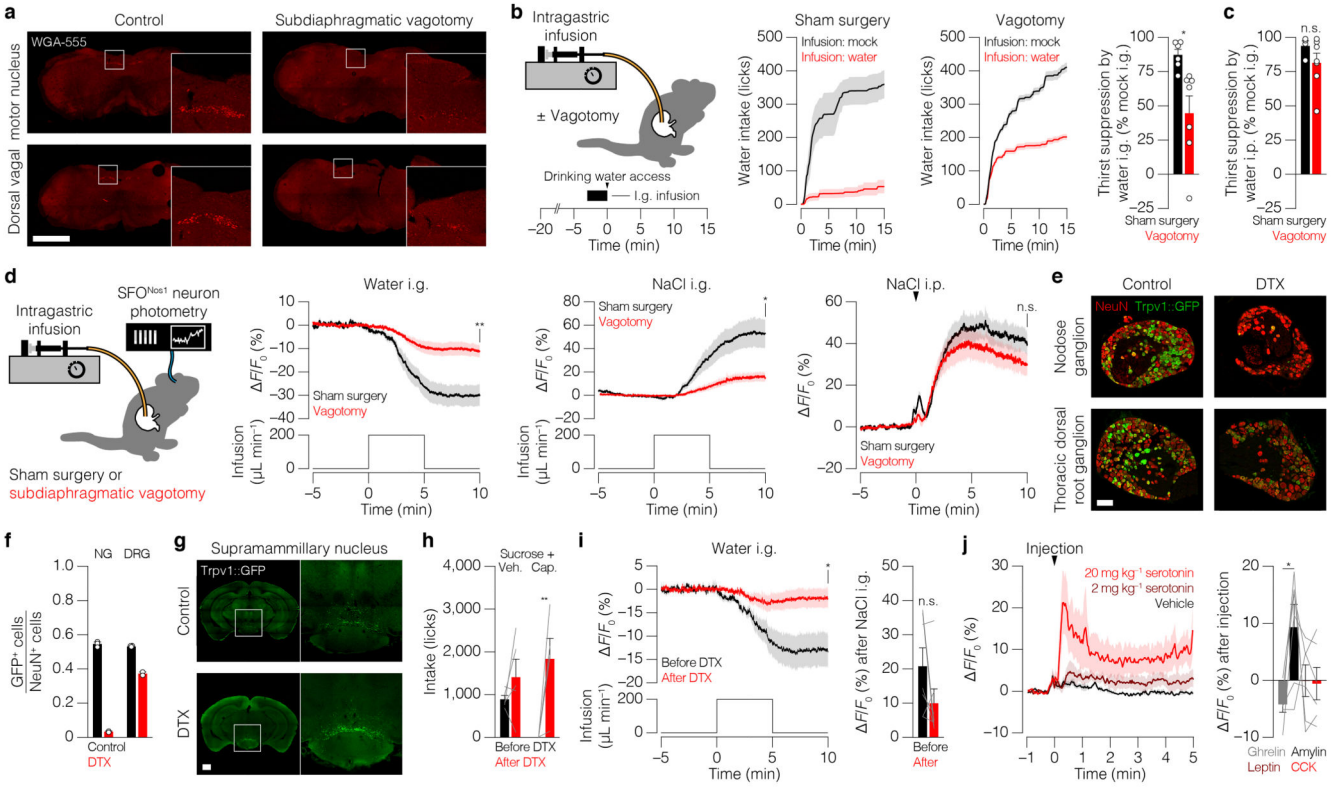

Extended Data Figure 4. The GI→SFO osmosensory signal involves the vagus nerve.

Panels **a–d** show that the GI→SFO osmosensory signal is disrupted by subdiaphragmatic vagotomy. **a,** Vagal motor neuron somas (located in the brainstem and labeled by i.p. injection of wheat germ agglutinin, WGA-555) were largely absent following subdiaphragmatic vagotomy (two examples per condition; scale bar, 1 mm). **b,** Drinking after dehydration was less suppressed by i.g. infusion of water in vagotomized mice (middle; $n = 7$ mice) compared to sham mice (left; $n = 6$ mice). Quantification (right; two-tailed Student's *t*-test). **c,** Drinking was similarly suppressed in both groups by systemic (i.p.) delivery of water ($n = 4$ sham and 7 vagotomy, two-tailed Student's *t*-test). **d,** SFO modulation by water and 500 mM NaCl i.g. infusions, but not by 1.5 M NaCl i.p. injection, was attenuated in vagotomized mice compared to sham mice ($n = 8$ mice per group, two-tailed Student's *t*-tests). Panels **e–i** show that the GI→SFO osmosensory signal involves *Trpv1*$^+$ sensory neurons. **e,** To specifically ablate *Trpv1*$^+$ sensory neurons, we treated mice containing a BAC transgene expressing GFP and the diphtheria toxin (DTX) receptor from the *Trpv1* gene start codon (*Trpv1-Gfp-2a-Dtr* mice) with DTX (scale bar, 100 μm). **f,** Quantification ($n = 3$ control and 2 DTX; NG, nodose ganglion; DRG, dorsal root ganglion). **g,** DTX treatment did not ablate *Trpv1*$^+$ neurons in the brain (scale bar, 1 mm). **h,** Hydrated mice avoided drinking 300 mM sucrose that contained 100 μM capsaicin (Cap.) before, but not after, DTX ablation of *Trpv1*$^+$ sensory neurons ($n = 5$ mice, two-way ANOVA, Holm-Šídák correction; Veh., vehicle). **i,** SFO modulation by water i.g. was significantly attenuated after DTX ablation of *Trpv1*$^+$ sensory neurons, and modulation by 500 mM NaCl i.g. was slightly attenuated ($n = 7$ mice, two-tailed Student's *t*-tests). Panel **j** shows the response of SFO neurons to serotonin and other visceral hormones. **j,** SFO neuron dynamics during

injection of two doses of serotonin (left; $n = 5$ mice) and to a single dose (2 mg kg^{-1}) of amylin, cholecystokinin (CCK), ghrelin, or leptin (right; $n = 6$ mice, one-way ANOVA, Holm-Šídák correction) in hydrated mice. Error bars and shaded areas represent mean ± s.e.m. *$P < 0.05$, **$P < 0.01$; n.s., not significant.

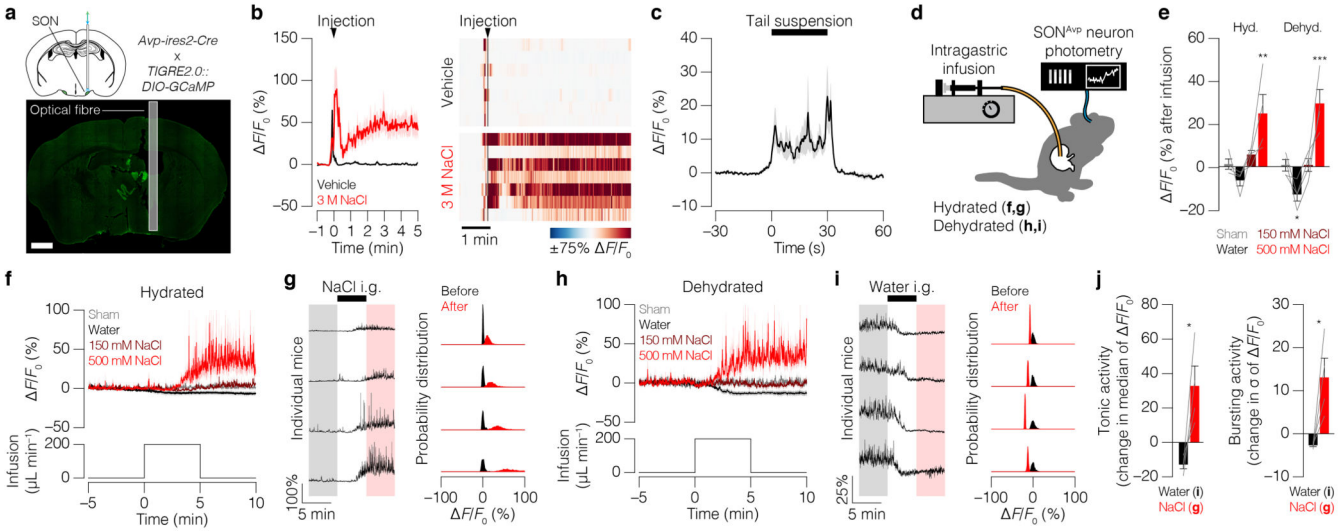

Extended Data Figure 5. Vasopressin neurons integrate systemic and GI osmosensory signals and are stress-responsive.

Panels **a,b** present additional data related to Fig. 3a,b. **a**, Schematic for fiber photometry recording of vasopressin neurons (scale bar, 1 mm). **b,** Vasopressin neuron dynamics (average, left; individual mice, right) during vehicle or NaCl i.p. injection ($n = 7$ mice). Panel **c** shows that vasopressin neurons are stress-responsive. **c,** Vasopressin neuron activity during tail suspension ($n = 7$ mice). Panels **d–j** present additional data related to Fig. 3d. **d,** Schematic. **e,** Vasopressin neuron activity change after infusion while hydrated or dehydrated ($n = 4$ mice, two-way ANOVA, Holm-Šídák correction; Hyd., hydrated; Dehyd., dehydrated). **f,** Vasopressin neuron activity during i.g. infusions while hydrated ($n = 4$ mice). **g,** Vasopressin neuron dynamics of individual mice (left) and distribution of $\Delta F/F_0$ values before and after 500 mM NaCl i.g. infusion for those mice (right). **h,** Vasopressin neuron dynamics during i.g. infusions after dehydration ($n = 4$ mice). **i,** Vasopressin neuron activity of individual mice (left) and distribution of $\Delta F/F_0$ values before and after water i.g. infusion for those mice (right). **j,** GI osmolarity modulates both the median of $\Delta F/F_0$ (left; used here as a proxy for tonic activity) and the standard deviation (σ) of $\Delta F/F_0$ (right; used here as a proxy for bursting activity) of vasopressin neurons ($n = 4$ mice, two-tailed Student's t-tests). Error bars represent mean ± s.e.m. Shaded areas in **b,c,f,h** represent mean ± s.e.m and in **g,i** represent "before" and "after" infusion periods. $*P < 0.05$, $**P < 0.01$, $***P < 0.001$.

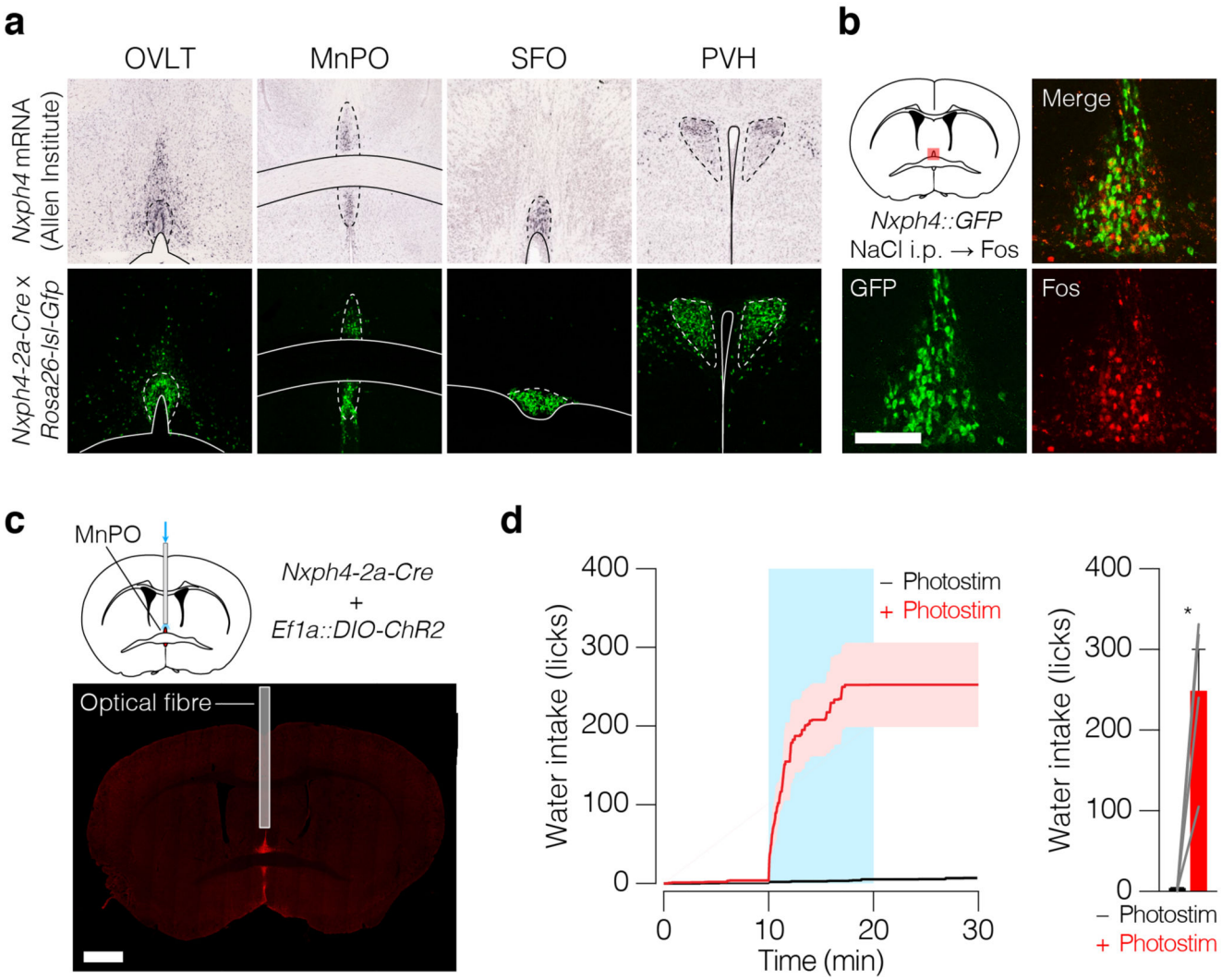

Extended Data Figure 6. *Nxph4*-expressing MnPO neurons are activated by dehydration and drive thirst.

Panel **a** presents additional data related to Fig. 4b. **a,** The *Nxph4–2a-Cre* recombination pattern (bottom; crossed to a GFP reporter line) recapitulates the endogenous *Nxph4* mRNA expression pattern (top; Allen Institute for Brain Science ISH #73521000) in the organum vasculosum of the lamina terminalis (OVLT), MnPO, SFO, and paraventricular hypothalamus (PVH). Panel **b** shows that MnPO^{Nxph4} neurons are activated by dehydration. **b,** *Nxph4-2a-Cre* recombination (green; crossed to a GFP reporter line) and the immediate early gene Fos (red; induced by 3 M NaCl i.p. injection) co-localize in the MnPO during dehydration (scale bar, 100 μm). Panels **c,d** show that MnPO^{Nxph4} neurons drive thirst. **c,** Schematic for optogenetic activation of MnPO^{Nxph4} neurons (scale bar, 1 mm). **d,** Water intake in response to photostimulation (left). Quantification (right; $n = 4$ mice, two-tailed Student's t-test). Error bars and shaded areas represent mean ± s.e.m. *$P < 0.05$.

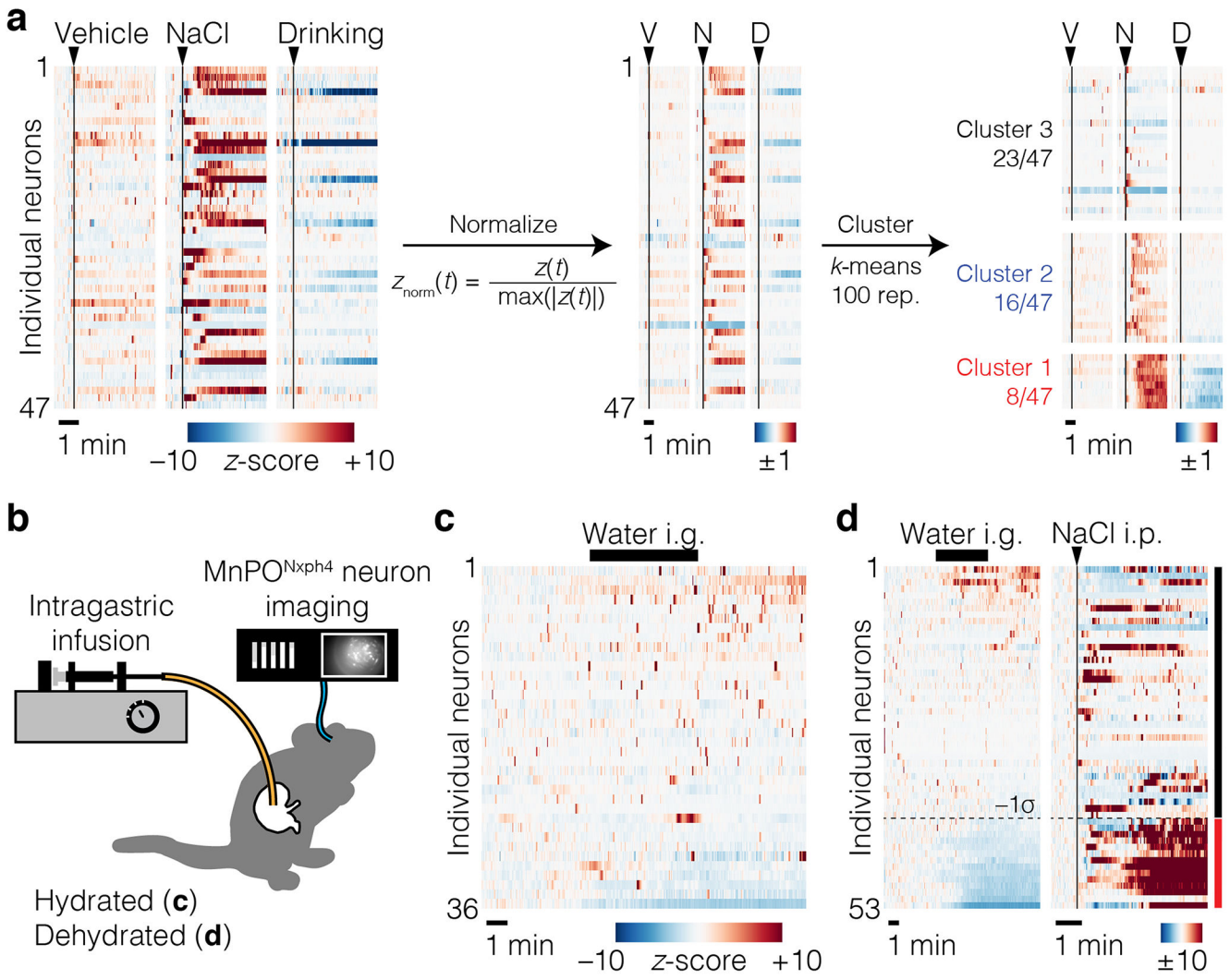

Extended Data Figure 7. *In vivo* imaging of individual glutamatergic MnPO neurons during thirst, drinking, and GI manipulation.

Panel **a** presents additional data related to Fig. 4d,e. **a,** Workflow for *k*-means clustering of individual MnPO^{Nxph4} neurons based on their activity during vehicle i.p. injection, 3 M NaCl i.p. injection, and water drinking. Panels **b–d** present additional data related to Fig. 4f–h. **b,** Schematic. **c,** Dynamics of individual neurons during water i.g. infusion while hydrated. **d,** Dynamics of individual neurons tracked during water i.g. infusion after dehydration (left) and 3 M NaCl i.p. injection (right). Neurons inhibited ≥1σ after water i.g. infusion were classified as “GI-tuned” (red; 26%) and the remaining neurons were classified as “GI-untuned” (black; 74%) for the time-course plotted in Fig. 4h.

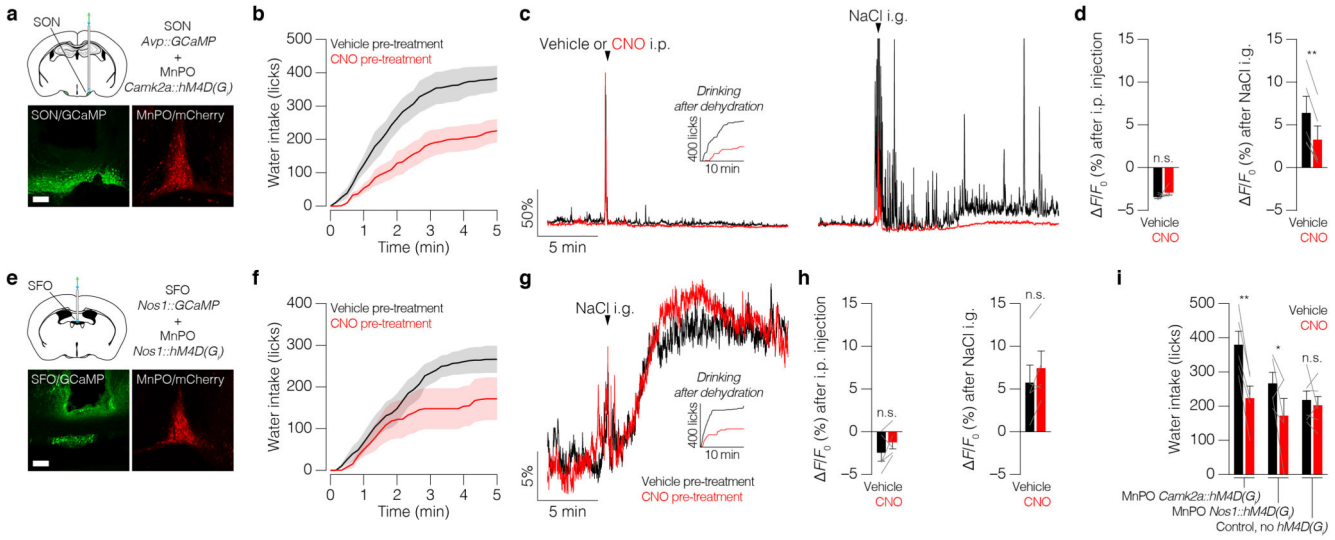

Extended Data Figure 8. Glutamatergic MnPO neurons relay the GI osmosensory signal to vasopressin neurons.

Panels **a–d** show that glutamatergic MnPO neurons are necessary for relaying GI osmosensory information to SON vasopressin neurons. **a,** Schematic for simultaneous fiber photometry recording of vasopressin neurons and chemogenetic inhibition of glutamatergic MnPO neurons (scale bar, 100 μm). **b,** Injection of clozapine *N*-oxide (CNO) inhibited water intake after dehydration ($n = 5$ mice). **c,** Example vasopressin neuron dynamics during CNO or vehicle i.p. injection (left) and subsequent 1.5 M NaCl i.g. by oral gavage (right). Inset, water intake after dehydration for this example mouse. **d,** Quantification of vasopressin neuron response to i.p. injection (left) and NaCl i.g. (right; $n = 5$ mice, two-tailed Student's *t*-tests). Panels **e–h** show that glutamatergic MnPO neurons are not necessary for relaying GI osmosensory information to SFO thirst neurons. **e,** Schematic for simultaneous fiber photometry recording of SFO neurons and chemogenetic inhibition of glutamatergic MnPO neurons (scale bar, 100 μm). **f,** Injection of CNO inhibited water intake after dehydration ($n = 5$ mice). **g,** Example SFO neuron dynamics during 1.5 M NaCl i.g. by oral gavage after CNO or vehicle i.p. injection. Inset, water intake after dehydration for this example mouse. **h,** Quantification of SFO neuron response to i.p. injection (left) and NaCl i.g. (right; $n = 5$ mice, two-tailed Student's *t*-tests). Panel **i** shows that CNO inhibits drinking in mice expressing hM4D(G_i) in glutamatergic MnPO neurons but not in control mice lacking hM4D(G_i). **i,** Injection of CNO significantly inhibited water intake after dehydration in $MnPO^{Camk2a::hM4D(Gi)}$ + SON photometry mice ($n = 5$ mice; quantified from panel **b**) and $MnPO^{Nos1::hM4D(Gi)}$ + SFO photometry mice ($n = 5$ mice; quantified from panel **f**) but not in control mice ($n = 6$ mice, two-way ANOVA, Holm-Šídák correction). Error bars and shaded areas represent mean ± s.e.m. $^*P < 0.05$, $^{**}P < 0.01$; n.s., not significant.

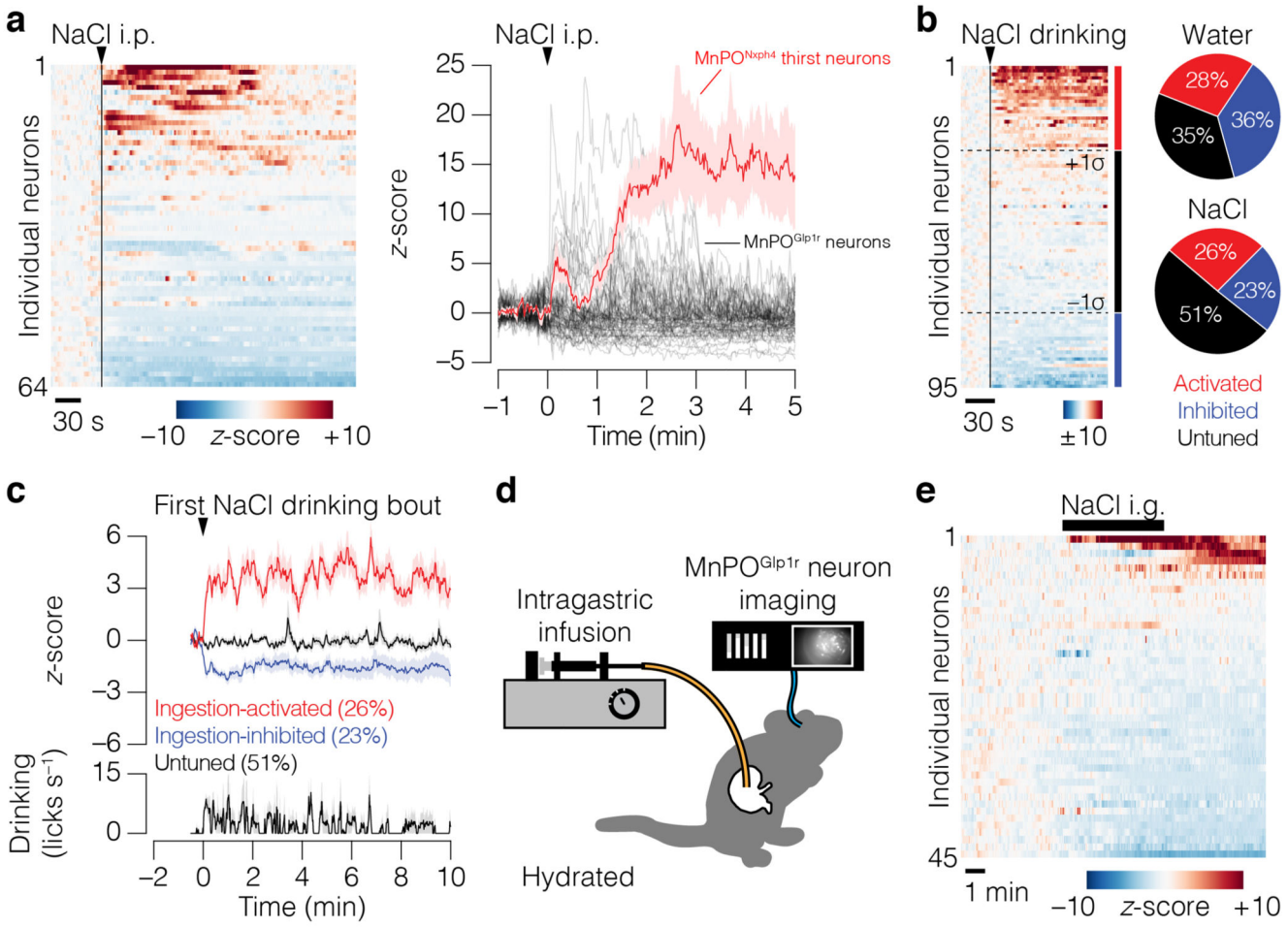

Extended Data Figure 9. ***In vivo*** **imaging of individual GABAergic MnPO neurons during thirst, drinking, and GI manipulation.**

Panel **a** shows that individual GABAergic MnPO neurons do not encode systemic osmolarity in their baseline activity. **a,** Dynamics of individual neurons during 3 M NaCl i.p. injection while hydrated (left). Comparison to thirst-activated MnPO^{Nxph4} neurons (right; "cluster 1" from Fig. 4e). Panels **b,c** show the dynamics of ingestion-tuned GABAergic MnPO neurons during hypertonic NaCl drinking. **b,** Dynamics of individual neurons during 300 mM NaCl drinking after dehydration (left). Proportion of ingestion-activated (red; modulated ≥1σ during first min of drinking), ingestion-inhibited (blue; modulated ≤–1σ), and untuned (black) neurons during water (top; n = 77 neurons from Fig. 5c,d) or 300 mM NaCl (bottom; n = 95 neurons) drinking (right). **c,** Average responses of ingestion-activated, ingestion-inhibited, and untuned neurons during 300 mM NaCl drinking (n = 95 neurons). Note that ingestion of NaCl persists for much longer than ingestion of water after dehydration (see Fig. 5d and Extended Data Fig. 1a), which may explain differences in the dynamics of ingestion-tuned GABAergic MnPO neurons when mice drink these fluids. Panels **d,e** present additional data related to Fig. 5e–g. **d,** Schematic. **e,** Dynamics of individual neurons during 500 mM NaCl i.g. infusion while hydrated.

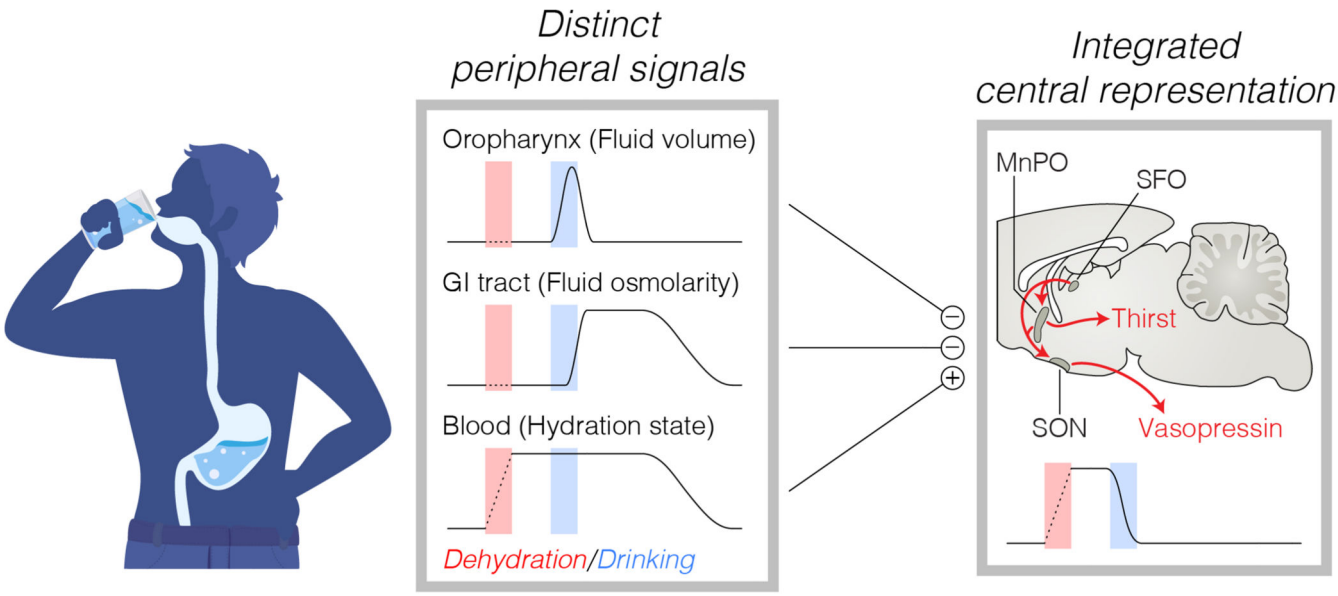

Extended Data Figure 10. Schematic for the neural control of thirst and satiation.

Anatomically and temporally distinct peripheral sensory signals encode information about the body's current hydration state (blood) as well as the volume (oropharynx) and osmolarity (GI tract) of recently ingested fluids. These signals converge on the brain's thirst circuit to generate an integrated central representation of fluid balance at the level of individual neurons, which use this information to dynamically control drinking behavior and vasopressin secretion in real-time. Illustration from iStock/artsholic.

Supplementary Material

Refer to Web version on PubMed Central for supplementary material.

Acknowledgements

C.A.Z. is supported by the NSF Graduate Research Fellowship (DGE-1144247), UCSF Discovery Fellowship, Genentech Foundation Predoctoral Fellowship, and NIH National Research Service Award (F31-HL137383). Z.A.K. is a Howard Hughes Medical Institute Investigator and is supported by the New York Stem Cell Foundation, American Diabetes Association, Rita Allen Foundation, McKnight Foundation, Alfred P. Sloan Foundation, Brain and Behavior Research Foundation, Esther A. and Joseph Klingenstein Foundation, UCSF Program for Breakthrough Biomedical Research, UCSF Diabetes Center, and UCSF Nutrition Obesity Research Center. This work was also supported by an NIH New Innovator Award (DP2-DK109533), R01-DK106399, and R01-NS094781. We thank the René Remie Surgical Skills Center for surgical training, Inscopix and Jones Parker for technical assistance, and members of the Knight lab for comments on the manuscript.

References

1. Zimmerman CA, Leib DE & Knight ZA Neural circuits underlying thirst and fluid homeostasis. Nat. Rev. Neurosci 18, 459–469, doi:10.1038/nrn.2017.71 (2017). [PubMed: 28638120]
2. Gizowski C & Bourque CW The neural basis of homeostatic and anticipatory thirst. Nat. Rev. Nephrol 14, 11–25, doi:10.1038/nrneph.2017.149 (2018). [PubMed: 29129925]
3. Johnson AK & Thunhorst RL The neuroendocrinology of thirst and salt appetite: visceral sensory signals and mechanisms of central integration. Front. Neuroendocrinol 18, 292–353, doi:10.1006/frne.1997.0153 (1997). [PubMed: 9237080]

4. McKinley MJ & Johnson AK The physiological regulation of thirst and fluid intake. News Physiol. Sci 19, 1–6, doi:10.1152/nips.01470.2003 (2004). [PubMed: 14739394]
5. Bellows RT Time factors in water drinking in dogs. Am. J. Physiol 125, 87–97, doi:10.1152/ajplegacy.1938.125.1.87 (1938).
6. Adolph EF, Barker JP & Hoy PA Multiple factors in thirst. Am. J. Physiol 178, 538–562, doi:10.1152/ajplegacy.1954.178.3.538 (1954). [PubMed: 13207374]
7. Thrasher TN, Nistal-Herrera JF, Keil LC & Ramsay DJ Satiety and inhibition of vasopressin secretion after drinking in dehydrated dogs. Am. J. Physiol. Endocrinol. Metabol 240, E394–E401, doi:10.1152/ajpendo.1981.240.4.e394 (1981).
8. Figaro MK & Mack GW Regulation of fluid intake in dehydrated humans: role of oropharyngeal stimulation. Am. J. Physiol. Regul. Integr. Comp. Physiol 272, R1740–R1746, doi:10.1152/ajpregu.1997.272.6.r1740 (1997).
9. Zimmerman CA et al. Thirst neurons anticipate the homeostatic consequences of eating and drinking. Nature 537, 680–684, doi:10.1038/nature18950 (2016). [PubMed: 27487211]
10. Mandelblat-Cerf Y et al. Bidirectional anticipation of future osmotic challenges by vasopressin neurons. Neuron 93, 57–65, doi:10.1016/j.neuron.2016.11.021 (2017). [PubMed: 27989461]
11. Allen WE et al. Thirst-associated preoptic neurons encode an aversive motivational drive. Science 357, 1149–1155, doi:10.1126/science.aan6747 (2017). [PubMed: 28912243]
12. Augustine V et al. Hierarchical neural architecture underlying thirst regulation. Nature 555, 204–209, doi:10.1038/nature25488 (2018). [PubMed: 29489747]
13. Weiner IH & Stellar E Salt preference of the rat determined by a single-stimulus method. J. Comp. Physiol. Psychol 44, 394–401, doi:10.1037/h0059237 (1951). [PubMed: 14861320]
14. Oka Y, Butnaru M, von Buchholtz L, Ryba NJP & Zuker CS High salt recruits aversive taste pathways. Nature 494, 472–475, doi:10.1038/nature11905 (2013). [PubMed: 23407495]
15. Maddison S, Wod RJ, Rolls ET, Rolls BJ & Gibbs J Drinking in the rhesus monkey: peripheral factors. J. Comp. Physiol. Psychol 94, 365–374, doi:10.1037/h0077664 (1980). [PubMed: 6767760]
16. Baertschi AJ & Vallet PG Osmosensitivity of the hepatic portal vein area and vasopressin release in rats. J. Physiol 315, 217–230, doi:10.1113/jphysiol.1981.sp013743 (1981). [PubMed: 7310708]
17. Stricker EM, Callahan JB, Huang W & Sved AF Early osmoregulatory stimulation of neurohypophyseal hormone secretion and thirst after gastric NaCl loads. Am. J. Physiol. Regul. Integr. Comp. Physiol 282, R1710–R1717, doi:10.1152/ajpregu.00548.2001 (2002). [PubMed: 12010753]
18. Gunaydin LA et al. Natural neural projection dynamics underlying social behavior. Cell 157, 1535–1551, doi:10.1016/j.cell.2014.05.017 (2014). [PubMed: 24949967]
19. Oka Y, Ye M & Zuker CS Thirst driving and suppressing signals encoded by distinct neural populations in the brain. Nature 520, 349–352, doi:10.1038/nature14108 (2015). [PubMed: 25624099]
20. Betley JN et al. Neurons for hunger and thirst transmit a negative-valence teaching signal. Nature 521, 180–185, doi:10.1038/nature14416 (2015). [PubMed: 25915020]
21. Ueno A et al. Mouse intragastric infusion (*iG*) model. Nat. Protoc 7, 771–781, doi:10.1038/nprot.2012.014 (2012). [PubMed: 22461066]
22. Andermann ML & Lowell BB Toward a wiring diagram understanding of appetite control. Neuron 95, 757–778, doi:10.1016/j.neuron.2017.06.014 (2017). [PubMed: 28817798]
23. Zhang F et al. Optogenetic interrogation of neural circuits: technology for probing mammalian brain structures. Nat. Protoc 5, 439–456, doi:10.1038/nprot.2009.226 (2010). [PubMed: 20203662]
24. Berthoud H-R & Neuhuber WL Functional and chemical anatomy of the afferent vagal system. Auton. Neurosci 85, 1–17, doi:10.1016/s1566-0702(00)00215-0 (2000). [PubMed: 11189015]
25. Vincent JD, Arnauld E & Bioulac B Activity of osmosensitive single cells in the hypothalamus of the behaving monkey during drinking. Brain Res 44, 371–384, doi:10.1016/0006-8993(72)90309-5 (1972). [PubMed: 4627634]

26. Abbott SBG, Machado NLS, Geerling JC & Saper CB Reciprocal control of drinking behavior by median preoptic neurons in mice. J. Neurosci 36, 8228–8237, doi:10.1523/jneurosci.1244-16.2016 (2016). [PubMed: 27488641]
27. Leib DE et al. The forebrain thirst circuit drives drinking through negative reinforcement. Neuron 96, 1272–1281, doi:10.1016/j.neuron.2017.11.041 (2017). [PubMed: 29268095]
28. McKinley MJ et al. The median preoptic nucleus: front and centre for the regulation of body fluid, sodium, temperature, sleep and cardiovascular homeostasis. Acta Physiol 214, 8–32, doi:10.1111/apha.12487 (2015).
29. Ghosh KK et al. Miniaturized integration of a fluorescence microscope. Nat. Methods 8, 871–878, doi:10.1038/nmeth.1694 (2011). [PubMed: 21909102]
30. Armbruster BN, Li X, Pausch MH, Herlitze S & Roth BL Evolving the lock to fit the key to create a family of G protein-coupled receptors potently activated by an inert ligand. Proc. Natl. Acad. Sci. USA 104, 5163–5168, doi:10.1073/pnas.0700293104 (2007). [PubMed: 17360345]
31. Bernard C Leçons de physiologie expérimentale appliquée à la médecine. (J.-B. Baillière et Fils, 1856).
32. Richter CP Total self regulatory functions in animals and human beings. Harvey Lecture Series 38, 63–103 (1943).
33. Cannon WB Organization for physiological homeostasis. Physiol. Rev 9, 399–431, doi:10.1152/physrev.1929.9.3.399 (1929).
34. Berridge KC Motivation concepts in behavioral neuroscience. Physiol. Behav 81, 179–209, doi:10.1016/j.physbeh.2004.02.004 (2004). [PubMed: 15159167]
35. Leshan RL, Greenwald-Yarnell M, Patterson CM, Gonzalez IE & Myers MGJ Leptin action through hypothalamic nitric oxide synthase-1–expressing neurons controls energy balance. Nat. Med 18, 820–823, doi:10.1038/nm.2724 (2012). [PubMed: 22522563]
36. Harris JA et al. Anatomical characterization of Cre driver mice for neural circuit mapping and manipulation. Front. Neural Circuits 8, 1–16, doi:10.3389/fncir.2014.00076 (2014). [PubMed: 24478635]
37. Williams EK et al. Sensory neurons that detect stretch and nutrients in the digestive system. Cell 166, 209–221, doi:10.1016/j.cell.2016.05.011 (2016). [PubMed: 27238020]
38. Zhou P et al. Interrogating translational efficiency and lineage-specific transcriptomes using ribosome affinity purification. Proc. Natl. Acad. Sci. USA 110, 15395–15400, doi:10.1073/pnas.1304124110 (2013). [PubMed: 24003143]
39. Daigle TL et al. A suite of transgenic driver and reporter mouse lines with enhanced brain-cell-type targeting and functionality. Cell 174, 465–480, doi:10.1016/j.cell.2018.06.035 (2018). [PubMed: 30007418]
40. Pogorzala LA, Mishra SK & Hoon MA The cellular code for mammalian thermosensation. J. Neurosci 33, 5533–5541, doi:10.1523/jneurosci.5788-12.2013 (2013). [PubMed: 23536068]
41. Yang H et al. One-step generation of mice carrying reporter and conditional alleles by CRISPR/Cas-mediated genome engineering. Cell 154, 1370–1379, doi:10.1016/j.cell.2013.08.022 (2013). [PubMed: 23992847]
42. Yang H, Wang H & Jaenisch R Generating genetically modified mice using CRISPR/Cas-mediated genome engineering. Nat. Protoc 9, 1956–1968, doi:10.1038/nprot.2014.134 (2014). [PubMed: 25058643]
43. Boyden ES, Zhang F, Bamberg E, Nagel G & Deisseroth K Millisecond-timescale, genetically targeted optical control of neural activity. Nat. Neurosci 8, 1263–1268, doi:10.1038/nn1525 (2005). [PubMed: 16116447]
44. Berndt A et al. High-efficiency channelrhodopsins for fast neuronal stimulation at low light levels. Proc. Natl. Acad. Sci. USA 108, 7595–7600, doi:10.1073/pnas.1017210108 (2011). [PubMed: 21504945]
45. Chen T-W et al. Ultrasensitive fluorescent proteins for imaging neuronal activity. Nature 499, 295–300, doi:10.1038/nature12354 (2013). [PubMed: 23868258]
46. Paxinos G & Franklin KB J. *The Mouse Brain in Stereotaxic Coordinates*. 4 edn, (Academic Press, 2012).

47. Beutler LR et al. Dynamics of gut-brain communication underlying hunger. Neuron 96, 461–475, doi:10.1016/j.neuron.2017.09.043 (2017). [PubMed: 29024666]
48. Höber R & Höber J Experiments on the absorption of organic solutes in the small intestine of rats. J. Cell. Comp. Physiol 10, 401–422, doi:10.1002/jcp.1030100402 (1937).
49. Mordes JP, el Lozy M, Herrera MG & Silen W Effects of vagotomy with and without pyloroplasty on weight and food intake in rats. Am. J. Physiol. Regul. Integr. Comp. Physiol 236, R61–R66, doi:10.1152/ajpregu.1979.236.1.r61 (1979).
50. Powley TL, Fox EA & Berthoud HR Retrograde tracer technique for assessment of selective and total subdiaphragmatic vagotomies. Am. J. Physiol. Regul. Integr. Comp. Physiol 253, R361–R370, doi:10.1152/ajpregu.1987.253.2.r361 (1987).
51. Powley TL, Chi MM, Baronowsky EA & Phillips RJ Gastrointestinal tract innervation of the mouse: afferent regeneration and meal patterning after vagotomy. Am. J. Physiol. Regul. Integr. Comp. Physiol 289, R563–R574, doi:10.1152/ajpregu.00167.2005 (2005). [PubMed: 15831767]
52. Resendez SL et al. Visualization of cortical, subcortical and deep brain neural circuit dynamics during naturalistic mammalian behavior with head-mounted microscopes and chronically implanted lenses. Nat. Protoc 11, 566–597, doi:10.1038/nprot.2016.021 (2016). [PubMed: 26914316]
53. Zhou P et al. Efficient and accurate extraction of *in vivo* calcium signals from microendoscopic video data. eLife 7, e28728, doi:10.7554/elife.28728 (2018). [PubMed: 29469809]
54. Sparta DR et al. Construction of implantable optical fibers for long-term optogenetic manipulation of neural circuits. Nat. Protoc 7, 12–23, doi:10.1038/nprot.2011.413 (2011). [PubMed: 22157972]
55. Krashes MJ et al. Rapid, reversible activation of AgRP neurons drives feeding behavior in mice. J. Clin. Invest 121, 1424–1428, doi:10.1172/jci46229 (2011). [PubMed: 21364278]
56. Roth BL DREADDs for neuroscientists. Neuron 89, 683–694, doi:10.1016/j.neuron.2016.01.040 (2016). [PubMed: 26889809]
57. Saito M et al. Diphtheria toxin receptor–mediated conditional and targeted cell ablation in transgenic mice. Nat. Biotechnol 19, 746–750, doi:10.1038/90795 (2001). [PubMed: 11479567]
58. Cavanaugh DJ et al. *Trpv1* reporter mice reveal highly restricted brain distribution and functional expression in arteriolar smooth muscle cells. J. Neurosci 31, 5067–5077, doi:10.1523/jneurosci.6451-10.2011 (2011). [PubMed: 21451044]

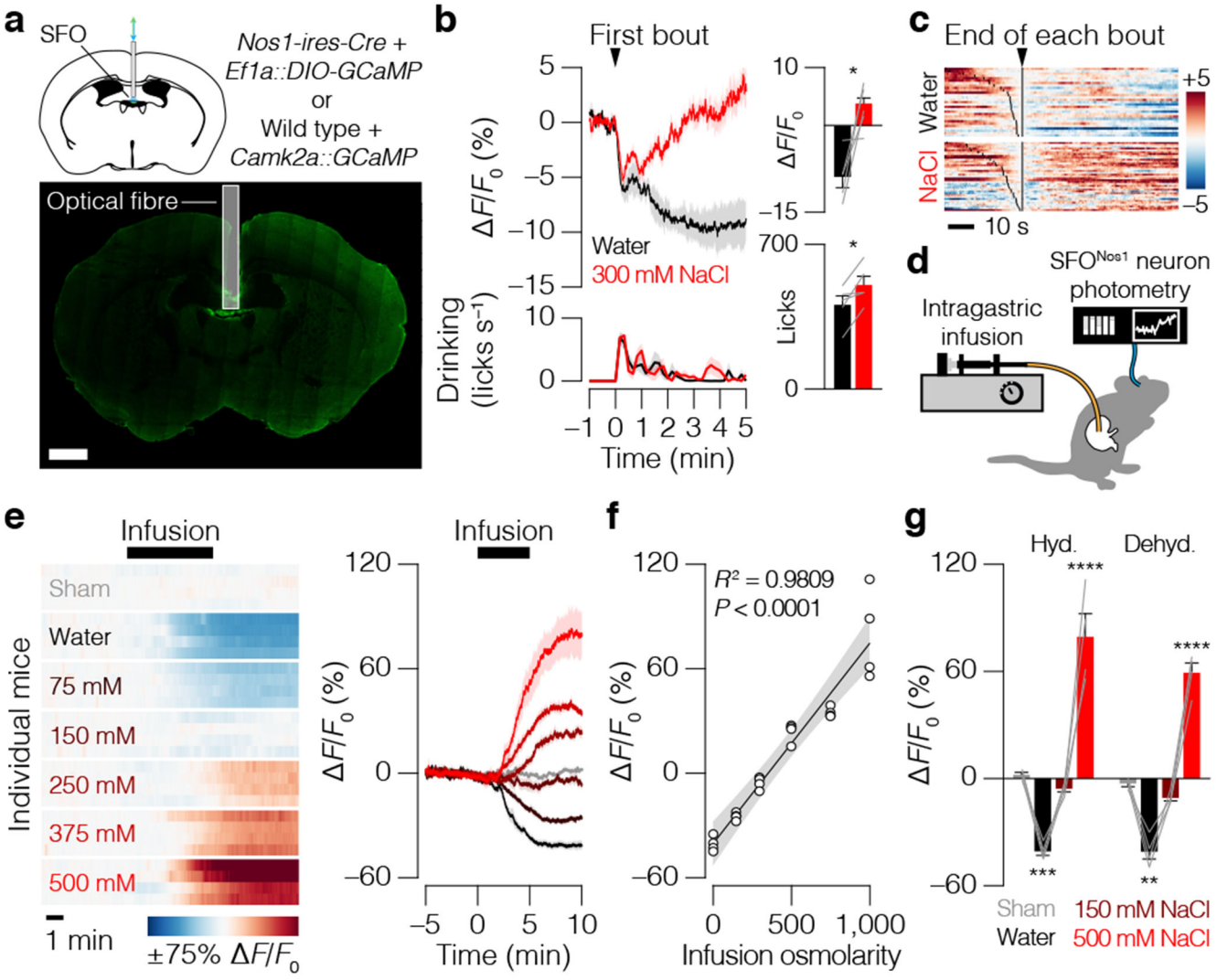

Figure 1. GI osmolarity modulates drinking behavior and SFO thirst neuron activity.

a, Schematic for fiber photometry recording of SFO neurons (scale bar, 1 mm). **b,** Average SFO activity and drinking behavior after dehydration (left). Quantification (right; $n = 5$ mice, two-tailed Student's t-tests). **c,** SFO neuron dynamics during individual water (29 bouts) or NaCl (37 bouts) drinking bouts. **d,** Schematic for i.g. infusion during fiber photometry recording. **e,** SFO neuron dynamics of individual mice during infusions of water or NaCl while hydrated (left). Average SFO activity during infusions (right; $n = 4$ mice). **f,** Correlation between infusion osmolarity (mOsm L^{-1}) and SFO activity change ($n = 4$ mice, linear regression). **g,** SFO activity change after infusion while hydrated or dehydrated ($n = 4$ mice, two-way ANOVA, Holm-Šídák correction; Hyd., hydrated; Dehyd., dehydrated). Error bars represent mean ± s.e.m. Shaded areas in **b,e** represent mean ± s.e.m. and in **f** represent 95% confidence interval of the line-of-best-fit. *$P < 0.05$, **$P < 0.01$, ***$P < 0.001$, ****$P < 0.0001$.

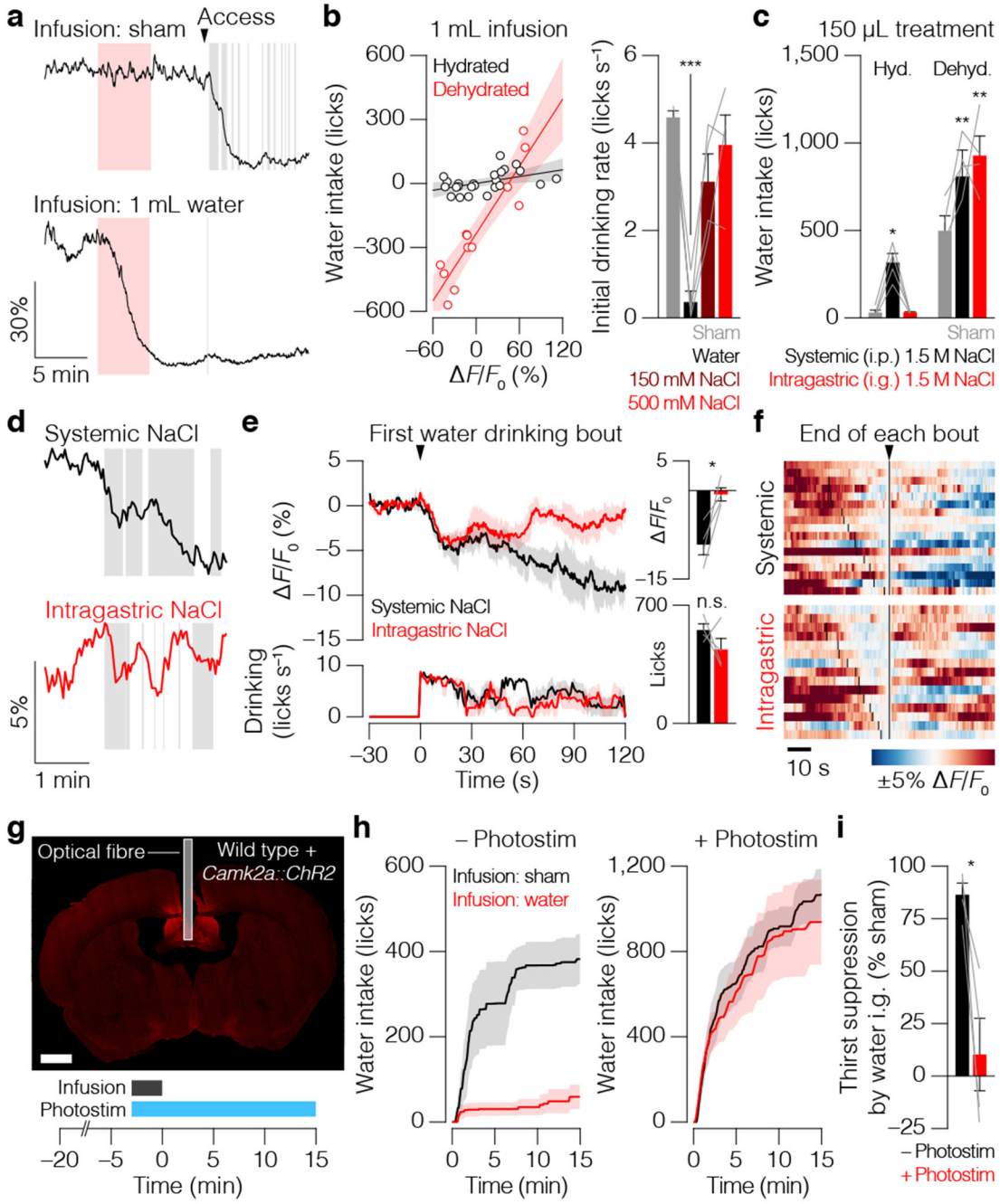

Figure 2. The GI→SFO osmosensory signal controls thirst satiation.

a, Example SFO neuron dynamics during i.g. infusion after dehydration. **b,** Correlation between SFO activity change and water intake (relative to sham infusion) after 1 mL infusions into hydrated (black; $n = 24$ experiments from 4 mice, linear regression, $R^2 = 0.2084$, $P = 0.0249$) or dehydrated (red; $n = 12$ experiments from 4 mice, linear regression, $R^2 = 0.8493$, $P < 0.0001$) mice (left). Initial drinking rate of dehydrated mice after infusion (right; $n = 4$ mice, one-way ANOVA, Holm-Šídák correction). **c,** Water intake after systemic (i.p.) or i.g. treatment with 150 µL NaCl (right; $n = 4$ mice, one-way ANOVA, Holm-Šídák

correction; Hyd., hydrated; Dehyd., dehydrated). **d,** Example SFO neuron dynamics during water drinking after 150 μL NaCl treatment into dehydrated mice. **e,** Average SFO activity and drinking behavior after 150 μL NaCl treatment into dehydrated mice (left). Quantification (right; $n = 4$ mice, two-tailed Student's *t*-tests). **f,** SFO neuron dynamics during individual water drinking bouts after systemic (17 bouts) or i.g. (15 bouts) 150 μL NaCl treatment. **g,** Schematic for i.g. infusion during optogenetic activation (scale bar, 1 mm). **h,** Dehydration-induced drinking after i.g. infusion either with (right) or without (left) simultaneous photostimulation of SFO neurons ($n = 4$ mice). **i,** Quantification ($n = 4$ mice, two-tailed Student's *t*-test). Error bars represent mean ± s.e.m. Shaded areas in **a,d** represent i.g. infusion (red) or individual licks (gray); in **b** represent 95% confidence interval of the line-of-best-fit; in **e,h** represent mean ± s.e.m. $*P < 0.05$, $**P < 0.01$, $***P < 0.001$; n.s., not significant.

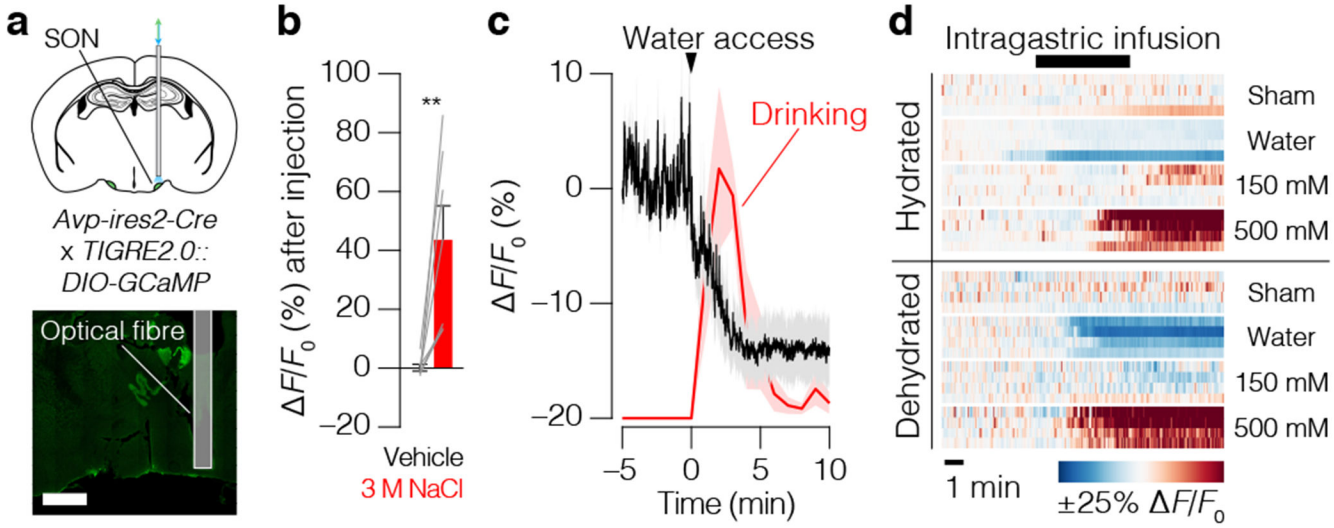

Figure 3. Vasopressin neurons bidirectionally encode GI osmolarity.

a, Schematic for fiber photometry recording of SON vasopressin neurons (scale bar, 1 mm). **b,** Vasopressin neuron response to vehicle or 3 M NaCl i.p. injection ($n = 7$ mice; two-tailed Student's t-test) **c,** Average vasopressin neuron activity and drinking behavior after dehydration ($n = 5$ mice). **d,** Vasopressin neuron dynamics of individual mice during i.g. infusions of water or NaCl ($n = 4$ mice). Error bars and shaded areas represent mean ± s.e.m.

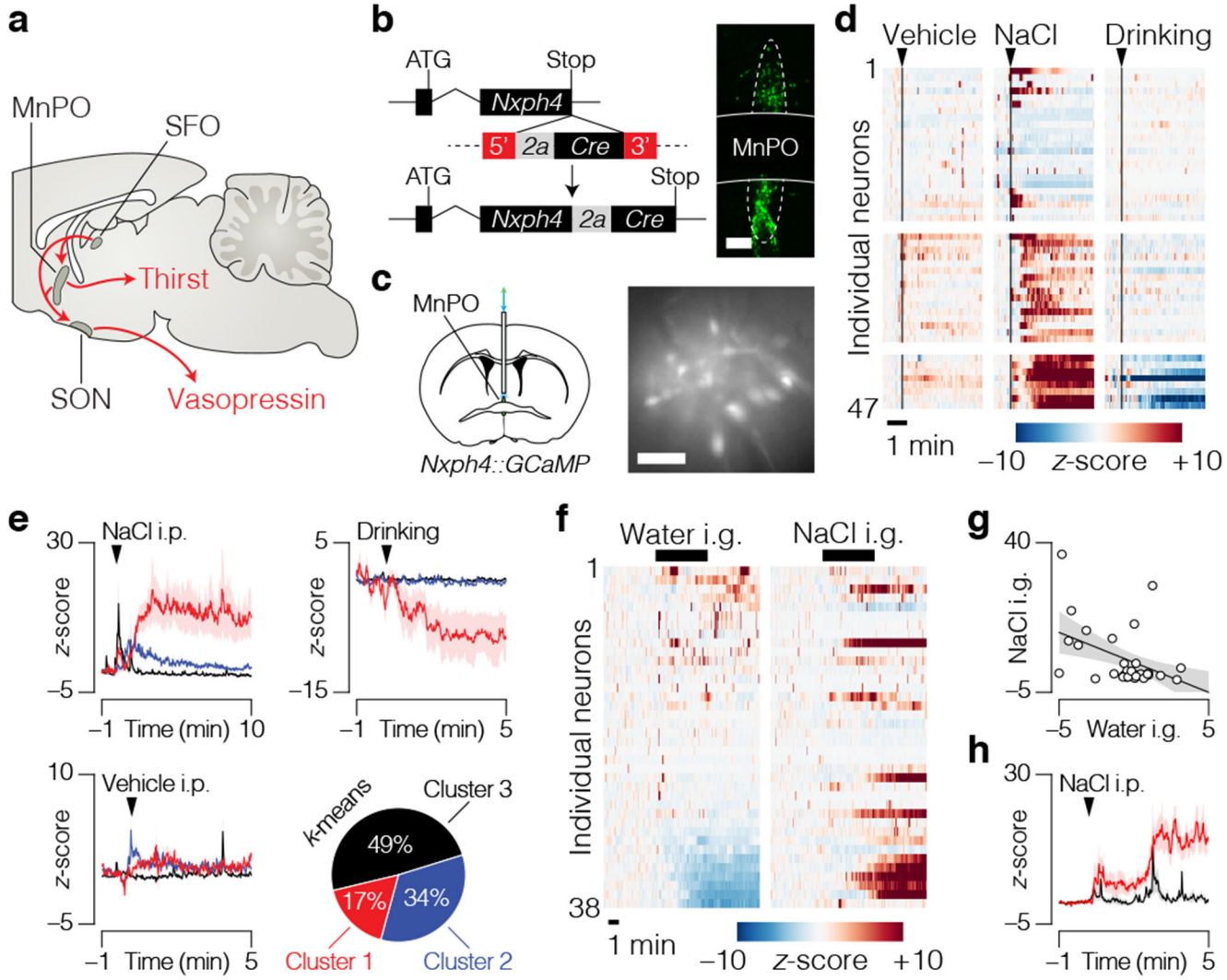

Figure 4. Individual glutamatergic MnPO neurons integrate information from the oropharynx, GI tract, and blood.

a, Illustration of the neural circuit that controls fluid homeostasis . **b,** Schematic for generation of the *Nxph4–2a-Cre* mouse line (left) and GFP-reporter recombination in the MnPO (right; scale bar, 100 μm). **c,** Schematic for microendoscope imaging of glutamatergic MnPO neurons (scale bar, 100 μm). **d,** Dynamics of individual neurons tracked during vehicle i.p. injection, 3 M NaCl i.p. injection, and water drinking. **e,** Average responses of neuron clusters (n = 47 neurons; see Extended Data Fig. 7a). **f,** Dynamics of individual neurons tracked during water i.g. infusion after dehydration (left) and during 500 mM NaCl i.g. infusion while hydrated (right). **g,** Correlation between the responses (z-score) of individual neurons to water i.g. and 500 mM NaCl i.g. (n = 38 neurons; linear regression, R^2 = 0.2154, P = 0.0033). **h,** Average response to 3 M NaCl i.p. injection of neurons that were inhibited (red; 26% inhibited ≥1σ after infusion) or un-modulated (black; 74%) by water i.g. infusion (n = 53 neurons; see Extended Data Fig. 7d). Shaded areas in time-courses represent mean ± s.e.m. and in regressions represent 95% confidence interval of the line-of-best-fit.

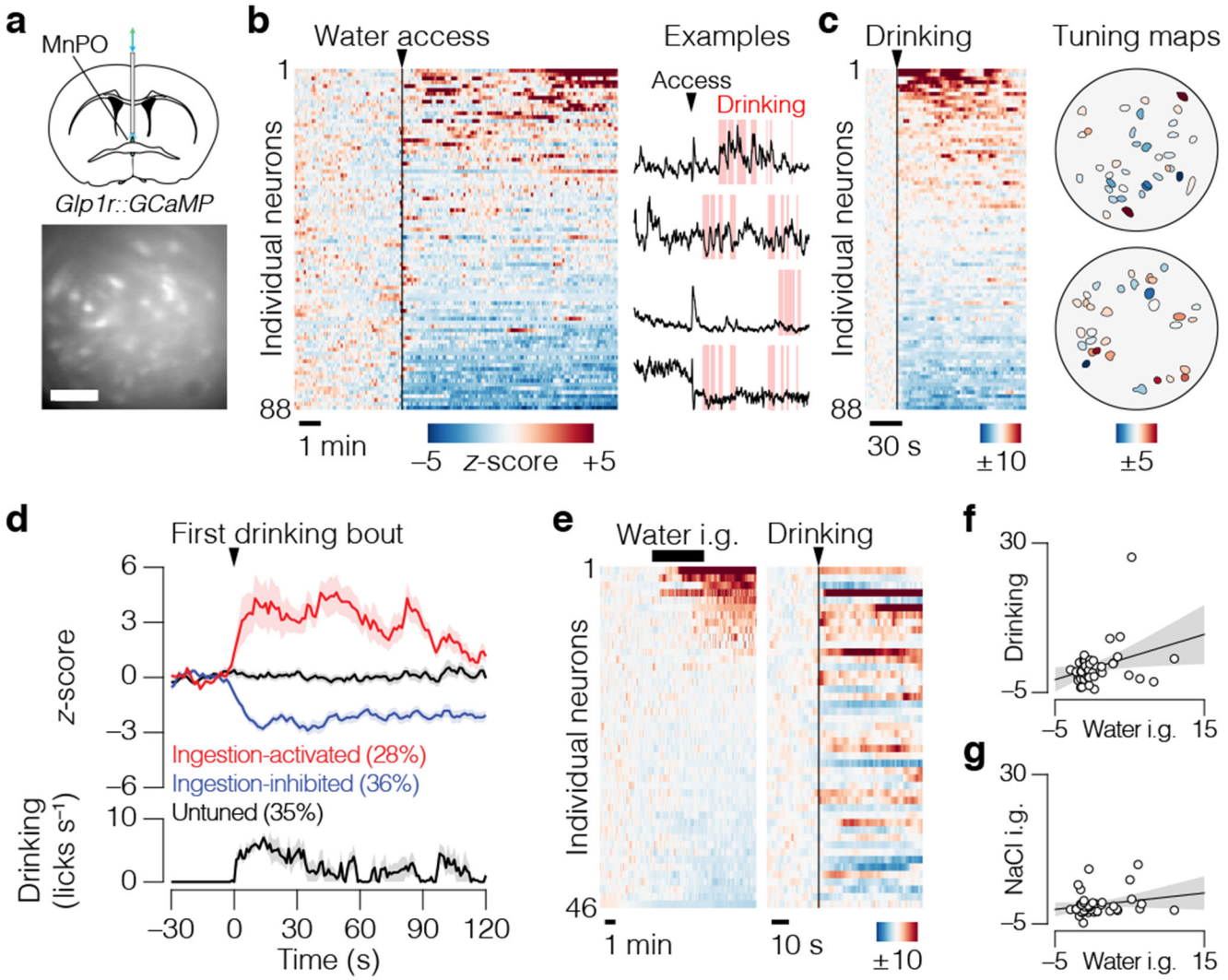

Figure 5. GABAergic MnPO neurons bidirectionally encode fluid ingestion.

a, Schematic for microendoscope imaging of GABAergic MnPO neurons (scale bar, 100 μm). **b,** Dynamics of individual neurons during water access after dehydration. **c,** Dynamics during drinking (left). Example tuning maps (right). **d,** Average responses of ingestion-activated (modulated ≥1σ during first min of drinking), ingestion-inhibited (modulated ≤–1σ), and untuned neurons during drinking (n = 77 neurons). **e,** Dynamics of individual neurons tracked during water i.g. infusion while hydrated (left) and during drinking after dehydration (right). **f,** Correlation between the responses (z-score) of individual neurons to water i.g. and drinking (n = 46 neurons; linear regression, R^2 = 0.1062, P = 0.0271). **g,** Correlation between the responses (z-score) to water i.g. and 500 mM NaCl i.g. (n = 45 neurons; linear regression, R^2 = 0.0467, P = 0.1514). Shaded areas in **b** represent individual licks; in **d** represent mean ± s.e.m.; in **f,g** represent 95% confidence interval of the line-of-best-fit.